Monthly Notices
of the
ROYAL ASTRONOMICAL SOCIETY

MNRAS **490,** 4447–4463 (2019)
Advance Access publication 2019 October 16

doi:10.1093/mnras/stz2887

Be it therefore resolved: cosmological simulations of dwarf galaxies with 30 solar mass resolution

Coral Wheeler,[1★] Philip F. Hopkins ,[1] Andrew B. Pace ,[2] Shea Garrison-Kimmel ,[1] Michael Boylan-Kolchin ,[3] Andrew Wetzel ,[4] James S. Bullock,[5] Dušan Kereš,[6] Claude-André Faucher-Giguère [7] and Eliot Quataert [8]

[1]TAPIR, Mailcode 350-17, California Institute of Technology, Pasadena, CA 91125, USA
[2]Mitchell Institute for Fundamental Physics and Astronomy, Department of Physics and Astronomy, Texas A&M University, College Station, TX 77843, USA
[3]Department of Astronomy, The University of Texas at Austin, 2515 Speedway, Stop C1400, Austin, TX 78712-1205, USA
[4]Department of Physics, University of California, Davis, CA 95616, USA
[5]Center for Cosmology, Department of Physics and Astronomy, University of California, Irvine, CA 92697, USA
[6]Department of Physics, Center for Astrophysics and Space Sciences, University of California at San Diego, 9500 Gilman Drive, La Jolla, CA 92093, USA
[7]Department of Physics and Astronomy and CIERA, Northwestern University, 2145 Sheridan Road, Evanston, IL 60208, USA
[8]Department of Astronomy and Theoretical Astrophysics Center, University of California Berkeley, Berkeley, CA 94720, USA

Accepted 2019 October 4. Received 2019 September 6; in original form 2018 November 30

ABSTRACT

We study a suite of extremely high-resolution cosmological Feedback in Realistic Environments simulations of dwarf galaxies ($M_{\rm halo} \lesssim 10^{10}\,{\rm M}_{\odot}$), run to $z = 0$ with $30\,{\rm M}_{\odot}$ resolution, sufficient (for the first time) to resolve the internal structure of individual supernovae remnants within the cooling radius. Every halo with $M_{\rm halo} \gtrsim 10^{8.6}\,{\rm M}_{\odot}$ is populated by a resolved *stellar* galaxy, suggesting very low-mass dwarfs may be ubiquitous in the field. Our ultra-faint dwarfs (UFDs; $M_{*} < 10^{5}\,{\rm M}_{\odot}$) have their star formation (SF) truncated early ($z \gtrsim 2$), likely by reionization, while classical dwarfs ($M_{*} > 10^{5}\,{\rm M}_{\odot}$) continue forming stars to $z < 0.5$. The systems have bursty star formation histories, forming most of their stars in periods of elevated SF strongly clustered in both space and time. This allows our dwarf with $M_{*}/M_{\rm halo} > 10^{-4}$ to form a dark matter core $>$200 pc, while lower mass UFDs exhibit cusps down to $\lesssim$100 pc, as expected from energetic arguments. Our dwarfs with $M_{*} > 10^{4}\,{\rm M}_{\odot}$ have half-mass radii ($R_{1/2}$) in agreement with Local Group (LG) dwarfs (dynamical mass versus $R_{1/2}$ and stellar rotation also resemble observations). The lowest mass UFDs are below surface brightness limits of current surveys but are potentially visible in next-generation surveys (e.g. LSST). The stellar metallicities are lower than in LG dwarfs; this may reflect pre-enrichment of the LG by the massive hosts or Pop-III stars. Consistency with lower resolution studies implies that our simulations are numerically robust (for a given physical model).

Key words: galaxies: dwarf – galaxies: formation – galaxies: kinematics and dynamics – Local Group – galaxies: star formation.

1 INTRODUCTION

Although the currently favoured cosmological paradigm – Λ cold dark matter (ΛCDM) theory – has been widely successful in predicting the counts, clustering, colours, morphologies, and evolution of galaxies on large scales, as well as a variety of cosmological observables (Eisenstein et al. 2005; Viel et al. 2008; Reid et al. 2010; Komatsu et al. 2011), several challenges have arisen to this model in recent years, most of them occurring at the smallest scales – those of dwarf galaxies ($M_{\star} \lesssim 10^{9}\,{\rm M}_{\odot}$; see e.g. Bullock & Boylan-Kolchin 2017 for a review.) Among these small-scale challenges, perhaps best known is the missing satellites problem (MSP; Klypin et al. 1999; Moore et al. 1999; Bullock 2010): counts of galaxies predicted from a naive assignment of stellar mass to dark-matter-only simulations of Milky Way (MW)-mass galaxies drastically overpredicts the actual number of currently observed dwarf galaxies around the MW.

The severity of the MSP is sensitive to the low-mass edge of galaxy formation: any halo mass threshold below which galaxy formation cannot proceed will result in firm predictions for the abundance and distribution of low-mass galaxies around the MW.

★ E-mail: coralrosewheeler@gmail.com

Published by Oxford University Press on behalf of the Royal Astronomical Society

In fact, Graus et al. (2018) suggest that the radial distribution of MW satellites requires galaxy formation to persist in dark matter haloes with virial temperatures below the atomic cooling limit, potentially presenting an issue in the opposite sense of the classic missing satellites problem.

Whether there is a well-defined halo mass scale at which galaxy formation ceases to operate, and the precise location of this low-mass cut-off, remain unknown. Any low-mass cut-off almost certainly would be affected by the timing of reionization – both the onset and the end – as well as by the overall flux of ionizing photons, the spectrum of the radiation, the proximity to more massive structure, and the self-shielding ability of the gas itself (Efstathiou 1992; Dijkstra et al. 2004; Hoeft et al. 2006; Weinmann et al. 2007; Oñorbe et al. 2015). Likewise, the properties of the lowest mass galaxies that do manage to form should reflect the imprint of the cosmic reionizing background. So-called 'fossils' of reionization, as first proposed by Ricotti & Gnedin (2005), are galaxies that managed to form some stars before having their star formation (SF) shut down by reionization (Bullock, Kravtsov & Weinberg 2000). Observations of six ultra-faint dwarfs (UFDs) around the MW show that they have stellar ages that are indistinguishable from ancient globular clusters, with the entirety of their SF occurring before $z \sim 2$ (Brown et al. 2014). This suggests that ultra-faint satellites of the MW are indeed fossils of the reionization era.

However, the fact that all of the UFDs considered in Brown et al. (2014) were satellites, rather than isolated galaxies, makes it more difficult to distinguish this effect from other quenching mechanisms, such as ram-pressure stripping (Gunn & Gott 1972). Wheeler et al. (2015, hereafter W15) used simulations run with the first-generation Feedback in Realistic Environments (FIRE; Hopkins et al. 2014)[1] and with baryonic particle masses $m^{\rm p}_{\rm bar} = 250\,{\rm M}_{\odot}$ to show that both isolated and satellite dwarfs in the UFD mass range had uniformly ancient stellar populations, suggesting that they were indeed reionization fossils. Additionally, Rodriguez Wimberly et al. (2018) removed haloes from dark-matter-only simulations (Garrison-Kimmel et al. 2014) that would have been destroyed by the galactic disc according to their pericentric distance (Garrison-Kimmel et al. 2017) and showed that there is a vanishingly small probability that all of the observed ultra-faints fell into the MW by $z = 2$, making environmental quenching an unlikely explanation for their ancient stellar ages.

Another well-known and long-standing small-scale challenge to ΛCDM is the core-cusp controversy (CCC; Flores & Primack 1994; Moore 1994; de Blok 2010), in which the predicted density of dark matter haloes as measured from dark-matter-only simulations suggests the presence of a central density 'cusp'[2] ($\rho \sim r^{-1}$; Navarro, Frenk & White 1997), while observations of some dwarf galaxies suggest that the actual profile shape can flatten at the centre, into a shallower density 'core' ($\rho \sim$ const; Salucci & Burkert 2000; van den Bosch & Dalcanton 2000; de Blok & Bosma 2002; Oh et al. 2008).

This issue has since been shown to be largely a result of comparing dark-matter-only simulations to observations, and that a dark matter core can be created in galaxies through repeated fluctuations in the gravitational potential via regular expulsions of the galactic gas supply from bursty SF and its resulting feedback (Mashchenko, Couchman & Wadsley 2006; Governato et al. 2012; Pontzen & Governato 2012; Chan et al. 2015; Oñorbe et al. 2015; Tollet et al. 2016). However, the ability of supernova (SN) feedback to reduce the central density of the dark matter halo is limited by the competing effects of the halo potential and the total mass in stars formed (Garrison-Kimmel et al. 2013). Galaxy formation is highly inefficient in the regime of UFDs ($M_\star \lesssim 10^5$), meaning the SN energy input per unit binding energy of the dark matter halo is much lower than in higher mass systems. Di Cintio et al. (2014a) showed that galaxies with $M_\star/M_{\rm vir} \lesssim 10^{-4}$ fail to produce enough SF to significantly alter the inner halo density cusp to a core. Indeed, most cosmological ΛCDM simulations to date fail to form cores in UFDs (Munshi et al. 2013; Fitts et al. 2017, although see Read, Agertz & Collins 2016a for an idealized study). Several UFDs have been found to host globular clusters near their centres, leading some authors to argue that their existence and the lack of dynamical friction implied is evidence for cores in these objects (Amorisco 2017; Caldwell et al. 2017), but there remains little direct observational evidence for cores in UFDs. If stronger evidence arises, it may require new physics in the dark sector (see e.g. Bullock & Boylan-Kolchin 2017; Buckley & Peter 2018; Tulin & Yu 2018, for recent reviews).

Our understanding of the severity of these challenges to ΛCDM is complicated by computational difficulties in dealing with low-mass galaxies. Most cosmological hydrodynamic simulations of dwarfs run to $z = 0$ – including smoothed particle hydrodynamics (SPH), moving-mesh, or adaptive mesh refinement (AMR) methods – have a quasi-Lagrangian mass resolution[3] in the range $\sim$250–$10^4\,{\rm M}_{\odot}$. This means that in UFDs, where the mass of the stellar content can be as low as only a few 100s of solar masses, these simulations may be unable to resolve the galaxies; if they do, these 'galaxies' often have very few, and sometimes even a single, star particles (Sawala et al. 2014; Wheeler et al. 2015; Munshi et al. 2017). This problem becomes more and more challenging at lower masses, because $M_\star/M_{\rm vir}$ drops rapidly (meaning a larger and larger number of resolution elements are required to represent the small number of stars that should be present at lower $M_{\rm vir}$).

As more and more UFDs are discovered and scrutinized at increasing levels of detail, it becomes imperative for cosmological hydrodynamic simulations to continue to push to higher resolution to allow for comparisons with observations. The stellar particle count must not only be large enough to ensure that the galaxy actually forms (i.e. is not a random grouping of non-gravitationally bound particles), but it also must be sufficient to accurately estimate, e.g. the half-light radius for the galaxies, as well as rotation or other higher order properties. Cosmological simulations must be able to reliably resolve UFDs to make firm predictions for the next generation of telescopes.

In this paper, we introduce a new set of high-resolution cosmological hydrodynamic zoom-in simulations (GIZMO/FIRE-2) of isolated dwarf galaxies with baryonic particle masses of $m^{\rm p}_{\rm bar} = 30\,{\rm M}_{\odot}$ – the highest resolution ever run to $z = 0$. This new generation of $m^{\rm p}_{\rm bar} \sim 10\,{\rm M}_{\odot}$ simulations marks a transition point between simulations that treat SF within a single stellar population in the aggregate and simulations that model the collapse and fragmentation of a molecular cloud into individual stars, and allows

---

[1] http://fire.northwestern.edu. FIRE uses the pressure–entropy version of SPH hydrodynamics.

[2] Note that Baushev & Pilipenko (2018) argue that the predictions of cusps themselves may be numerical artefacts.

[3] Mass resolution is set by a combination of e.g. the numerical cell/particle masses and the physical minimum gas mass at which a self-gravitating structure can be identified, which are similar in our study but do not have to be in general (see Hopkins et al. 2018b).

us to probe smaller physical scales than previously possible in cosmological simulations. This in turn enables the comparison between a larger set of 'resolved' simulated UFDs and an ever-increasing set of observations at the low-mass end of galaxy formation. We introduce the suite in Section 2, give an overview of results and compare to observations in Section 3, including the star formation histories (SFHs, Section 3.2), halo structure (Section 3.3), kinematics (Section 3.4), and chemical abundances (Section 3.5). We conclude in Section 5.

2 SIMULATIONS

2.1 Resolution and motivation

Our highest resolution suite consists of cosmological zoom-in simulations of Lagrangian volumes surrounding three 'primary' isolated dwarf galaxy haloes (m10q$_{30}$, m10v$_{30}$, m09$_{30}$), each with baryonic particle mass of $m^{\rm p}_{\rm bar} = 30\,{\rm M}_{\odot}$ ($m_{\rm dm}$ is larger by $\Omega_{\rm m}/\Omega_{\rm b}$), and $z = 0$ virial masses[4] $\sim$2–10 × $10^9\,{\rm M}_{\odot}$ (see Table 1 for a full list of simulation properties).

Before going forward, we stress that the mass resolution achieved here, $\sim$30 M$_{\odot}$, is not simply an incremental improvement. It reaches a critical physical scale where the cooling radius of an SN remnant (approximately the radius enclosing $\sim$3000 M$_{\odot}$, with only very weak residual dependence on metallicity or gas density) is resolved with $\gtrsim$100 elements, which is essential for capturing the basic dynamics. Furthermore, many independent studies (e.g. Lapi, Cavaliere & Menci 2005; Kim & Ostriker 2015; Martizzi, Faucher-Giguère & Quataert 2015; Walch & Naab 2015; Hu 2018; Hopkins et al. 2018a) have shown that with mass resolution of $\lesssim$100 M$_{\odot}$, predictions for SN feedback become nearly independent of the detailed numerical implementation: whether one simply 'dumps' $\sim10^{51}$ erg into surrounding gas in thermal or energy, or applies a more sophisticated injection model, the asymptotic behaviour of the blastwave will converge to the same behaviour at this resolution. As a result, Hopkins et al. (2018a) showed the predictions of galaxy-formation simulations become vastly less-sensitive to the sub-grid model for feedback. We will therefore compare various properties at our high resolution and a resolution approximately eight times poorer. In Hopkins et al. (2018b), the primary galaxies m10q$_{30}$ and m10v$_{30}$ are also studied at even lower resolution.

2.2 Numerical methods

All details of the numerical methods and initial conditions[5] are presented in Hopkins et al. (2018b), where lower resolution versions of these volumes were studied extensively. We briefly summarize essential elements here.

The simulations are run with the GIZMO (Hopkins 2014)[6] code using the updated FIRE-2 implementation of SF and stellar feedback from Hopkins et al. (2018b). FIRE-2 uses the 'meshless finite mass' (MFM) Lagrangian finite-volume Godunov method for the hydrodynamics, accounts for gas heating from a variety of processes including the UV background[7] and local sources and cooling from $T = 10$–10^{10} K. As in all FIRE-2 simulations, we model SF via a sink-particle method in gas that is locally self-gravitating, Jeans-unstable, self-shielding/molecular, and exceeds a critical density $n_{\rm crit}$ (see Table 1). Details of the SF prescription can be found in Hopkins et al. (2018b). We adopt a standard, flat ΛCDM cosmology with $h \approx 0.70$, $\Omega_{\rm m} = 1 - \Omega_{\Lambda} \approx 0.27$, and $\Omega_{\rm b} \approx 0.045$ (consistent with current constraints; see Planck Collaboration XVI 2014).[8]

Once stars form, stellar feedback from SNe (Ia & II), stellar mass-loss (O/B and AGB), and radiation (photoelectric and photoionization heating, and radiation pressure, with a five-band radiation transport algorithm; see Hopkins et al. 2018a) are included following a STARBURST99 stellar evolution model (Leitherer et al. 1999) based on the star particle age and metallicity [adopting a Kroupa 2002 initial mass function (IMF)]. In lower resolution simulations, the feedback quantities (e.g. SNe rates, stellar spectra) can simply be IMF averaged. At the high resolution here, however, this produces un-physical outcomes: for example, it effectively assigns an expectation value of $\sim$1/3 of an O-star to each new star particle, rather than having $\sim$1/3 of star particles in young stellar populations contain an expectation value of one O-star. We therefore follow Ma et al. (2015), Su et al. (2018b), and Grudić & Hopkins (2018) by scaling all IMF-averaged feedback rates that depend on O-stars (i.e. photoionization and photoelectric heating, UV radiation pressure, OB winds, and core-collapse SNe) by the 'O-star number', which is discretely sampled from a Poisson distribution with expectation value $< N_0 > \approx m^{\rm p}_{\rm bar}/100\,{\rm M}_{\odot}$ at the time a star particle first forms, and then reduced by one each time a core-collapse SN occurs in that particle. Done in this manner, the IMF average is recovered when summing over the entire population. Note that while Su et al. (2018b) show in a variety of tests that this has little effect on galaxy properties when compared to run-to-run stochastic variation, Applebaum et al. (2018) show that stochastic sampling of the IMF makes feedback burstier, stronger, and quenches SF earlier in small dwarf galaxies.

2.3 Analysis

We use the Amiga Halo Finder (AHF; Knollmann & Knebe 2009) to identify gravitationally bound members of each halo in post-processing. We initially require >100 bound *star* particles to consider a galaxy resolved. Because AHF can incorrectly assign central stellar halo stars to subhaloes, we visually inspected each simulation to determine whether all star particles within the virial radius of each halo are physically associated with the central galaxy or with a satellite, in some cases adjusting the radial extent, $r^*_{\rm max}$, and stellar mass of the galaxy accordingly. All figures reflect these adjustments. Table 1 summarizes the properties of all dwarfs that meet this criterion. Note that a less conservative $\sim$15-particle cut yields >100 additional galaxies; these will be studied in future work.

---

[4] We define virial overdensity with the spherical top hat approximation of Bryan & Norman (1998).

[5] The ICs used here are publicly available at http://www.tapir.caltech.edu/ phopkins/publicICs

[6] A public version of GIZMO is available at http://www.tapir.caltech.edu/ phopkins/Site/GIZMO.html

[7] We adopt the UV background from the 2011 December update of Faucher-Giguère et al. (2009) (available here: http://galaxies.northwestern.edu/uvb/), which reionizes the Universe rapidly around $z \sim 10$ and completes reionization by $z = 6$, and was designed to produce a reionization optical depth consistent with WMAP-7.

[8] For the sake of comparison with other work using lower resolution versions of the same halo, m09$_{30}$ adopts slightly different cosmological parameters than the other two simulations. These differences are at the $\sim$1 per cent level, and matter far less than stochastic run-to-run variance.

Table 1. Properties of dwarfs in the suite. Each row lists a different *resolved, central or satellite* galaxy at $z = 0$. Columns give: (1) $M_{\rm halo}$: halo mass. (2) $R_{\rm vir}$: virial radius. (3) $V_{\rm max}$: maximum circular velocity. (4) M_*: bound stellar mass after removal of satellites and contamination. (5) $R_{\rm max}$: radial extent of stars (maximum radius of *any* bound star), as determined from visual inspection. (6) $R_{1/2}$: mean projected (2D) half-stellar-mass radius. (7) $v_{\rm rot}/\sigma$: ratio of the stellar velocity shear $v_{\rm rot}$ to dispersion σ. (8) $g_{\rm soft}$: typical minimum gas gravitational + hydrodynamic force softening reached in star-forming gas (this is adaptive). (9) DM$_{\rm soft}$: dark matter force softening (held constant). (10) $n_{\rm crit}$: minimum gas density required for SF (in addition to self-shielding, Jeans instability, and self-gravity).

	$M_{\rm halo}(10^9\,{\rm M}_\odot)$	$r_{\rm vir}$(kpc)	$V_{\rm max}$ (kms^{-1})	$M_\star(10^3\,{\rm M}_\odot)$	$r^*_{\rm max}$ (kpc)	$R_{1/2}$ (pc)	$v_{\rm rot}/\sigma$	g$_{\rm soft}$ (pc)	DM$_{\rm soft}$ (pc)	$n_{\rm crit}$(cm^{-3})
Resolved central galaxies in our high-resolution (30 M$_\odot$) simulations (>100 star particles in AHF-identified halo)										
m10q$_{30}$	7.7	51	34	5200	7.7	720	0.17	0.40	14	1000
m10q$_{30}$ Sat	0.34	6.3	16	1.2	1.2	560	0.85	0.40	14	1000
m10v$_{30}$	9.0	54	30	330	8.2	330	0.45	0.10	14	1e5
m10v$_{30}$ B	3.2	37	24	41	5.6	280	0.20	0.10	14	1e5
m10v$_{30}$ C	1.1	26	16	2.9	3.9	540	0.39	0.10	14	1e5
m10v$_{30}$ D	0.75	24	16	3.7	4.8	860	0.37	0.10	14	1e5
m10v$_{30}$ Sat	0.52	20	13	2.0	2.8	430	0.29	0.10	14	1e5
m10v$_{30}$ F	0.44	20	12	1.9	2.5	560	0.66	0.10	14	1e5
m10v$_{30}$ G	0.27	17	12	2.3	2.5	570	1.1	0.10	14	1e5
m09$_{30}$	2.5	35	22	12	4.0	200	0.56	0.10	14	1e5
m09$_{30}$ B	0.67	23	15	1.8	3.4	620	0.79	0.10	14	1e5
Resolved central galaxies in our standard-resolution (250 M$_\odot$) simulations (>100 star particles in AHF-identified halo)										
m10q$_{250}$	7.5	51	34	2700	7.7	550	0.19	1.0	29	1000
m10v$_{250}$	8.4	53	30	300	8.0	310	0.31	1.0	29	1000
m10v$_{250}$ B	2.7	37	24	66	5.5	350	0.14	1.0	29	1000
m09$_{250}$	2.5	36	22	27	5.3	420	0.14	1.0	29	1000

3 RESULTS

Fig. 1 shows the DM and stellar distribution in the primary galaxies of each of our zoom-in simulations as well as in the satellites of m10q (only resolved at the highest resolution) and m10v. The gas surface density and temperature maps for the same galaxies are shown in Figs 2–3. In order to best illustrate the structure in each over a relatively small range in each quantity, the density and temperature scales are different for each galaxy. In general, there is more structure visible in the $M_{\rm halo} \sim 10^{10}\,{\rm M}_\odot$ haloes than in m9, which is what we would expect due to the fact that m9 ceased SF at high redshift, and so the gas exists near the UV background temperature. The low gas density and high gas temperature of m10q$_{30}$ (bottom left) is a result of a particular event – a mini-burst of SNe that suppresses the SF at $z \sim 0.5$. We discuss this further in Section 3.2.

In general, there is not a significant difference in the appearance of the gas in the galaxies as a function of resolution. This is a result of the relatively low density of the gas at late times in these dwarfs. Because the code is Lagrangian, effective resolution scales with the local density, i.e. $g_{\rm soft} \sim (3\,{\rm pc})(\frac{m^{\rm p}_{\rm bar}}{30\,{\rm M}_\odot})^{1/3}(\frac{n_{\rm crit}}{1\,{\rm cm}^{-3}})^{-1/3}$. At median interstellar medium (ISM) densities of $n_{\rm crit} \sim 1\,{\rm cm}^{-3}$, the effective resolution is ∼3 pc, while at the very high densities required for SF, $n_{\rm crit} \sim 10^4$–$10^5\,{\rm cm}^{-3}$, the effective resolution is ∼0.1 pc. So while the benefits of the increased spatial resolution are significant in dense star-forming gas, only one galaxy at our highest resolution (m10v$_{30}$, bottom centre) has any ongoing SF at $z = 0$, and so the improved resolution is not highly visible in the images.

3.1 Halo and stellar masses

Fig. 4 compares the stellar mass–halo mass relation of the simulations for all galaxies in the high-resolution region we consider well resolved to observational constraints implied by abundance matching (AM). First, we note that while stochastic run-to-run variations (e.g. the magnitude of the largest starbursts at high redshift; see El-Badry, Weisz & Quataert 2017; Su et al. 2018a, b; Keller et al. 2019) can lead to changes as large as a factor approximately two in M_*, there does not appear to be any *systematic* dependence on resolution between our $m^{\rm p}_{\rm bar} = 250\,{\rm M}_\odot$ and $m^{\rm p}_{\rm bar} = 30\,{\rm M}_\odot$ runs in these properties for the approximately four galaxies that are well resolved at both resolution levels. We have also run volumes m10v and m10q at even lower resolution; at resolution $(30,\ 250,\ 2 \times 10^3,\ 1.6 \times 10^4,\ 1.3 \times 10^5)\,{\rm M}_\odot$, the primary galaxy in m10v has stellar mass $M_* = (3.3,\ 3.0,\ 1.5,\ 4.8,\ 2.6) \times 10^5\,{\rm M}_\odot$, and the primary in m10q has $M_* = (5.2,\ 2.7,\ 3.0,\ 2.0,\ 1.3) \times 10^6\,{\rm M}_\odot$. This suggests the sub-grid algorithm that couples SNe mass, energy, and momentum to surrounding gas particles properly handles the transition between explicitly resolved and unresolved SNe remnants, as it is specifically designed to do (see Hopkins et al. 2018a for extensive tests and discussion). That, in turn, is encouraging for the robustness of previous (lower resolution) predictions from FIRE simulations.

The grey circles in Fig. 4 are simulated galaxies from W15, run with FIRE-1 physics[9] at $m^{\rm p}_{\rm bar} = 250\,{\rm M}_\odot$ resolution. Although the UFDs simulated at this resolution had only tens of star particles, both these and the higher mass dwarfs have stellar masses consistent with the results presented here. This is in line with results at higher mass showing consistency between results from both versions of the FIRE code (Hopkins et al. 2018b).

Our simulated galaxies broadly sample the scatter about extrapolated AM relationships that are tuned to reproduce the stellar mass function of the Local Group (LG; Garrison-Kimmel et al. 2014 & Brook et al. 2014), suggesting that the underlying prescriptions in our runs should also reproduce observations when applied to LG-like environments at this resolution. However we stress this comparison is not rigorous: almost all of the simulated galaxies are

---

[9] For a list of changes between FIRE-1 and FIRE-2, see Hopkins et al. (2018b).

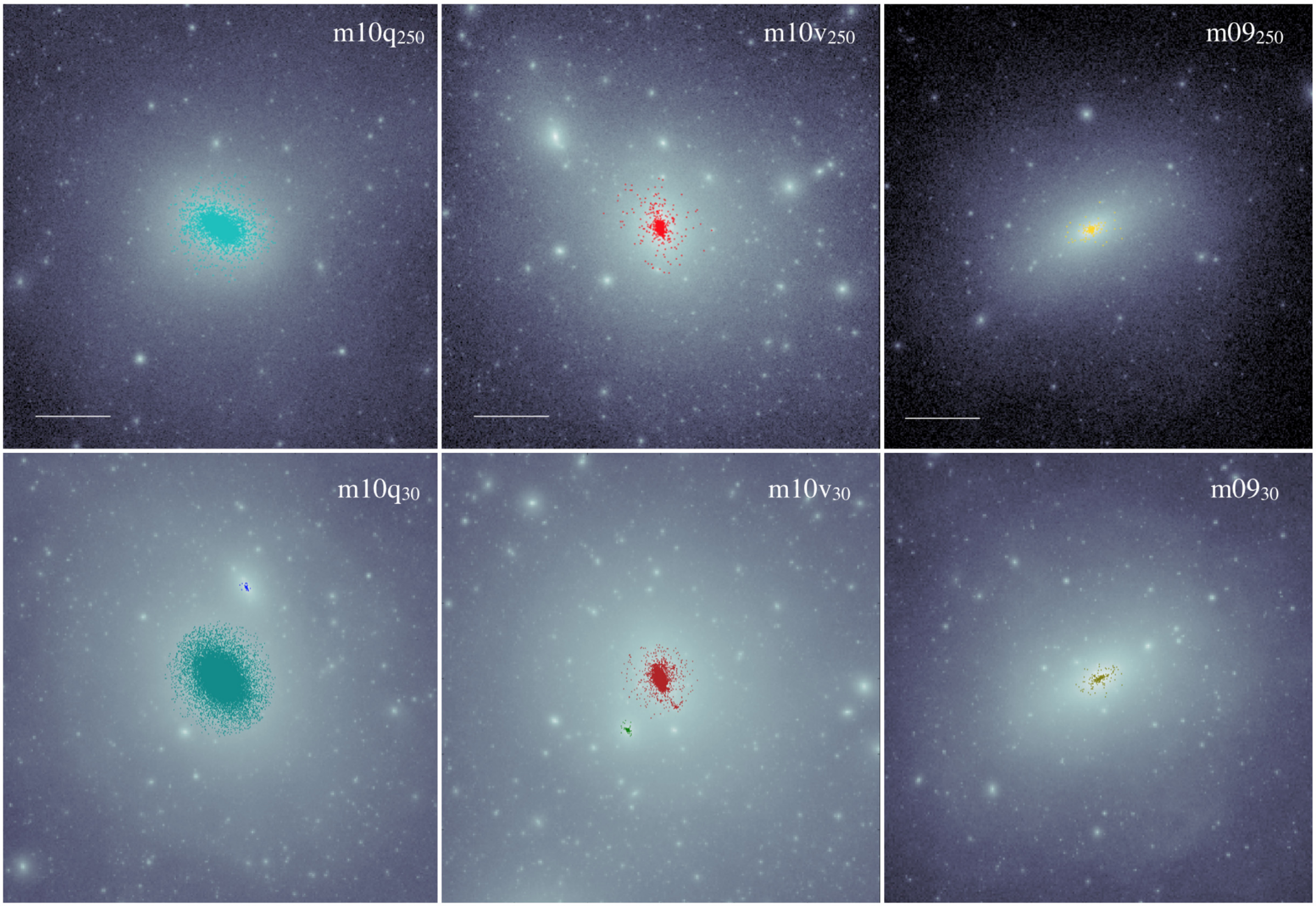

Figure 1. Dark matter density distribution (grey-scale) within the central 30 kpc for each simulation in Table 1, along with star particles (colours for each simulation) belonging to the central galaxy or a satellite (within $r^{*}_{\rm max}$; see Table 1). The top panels show galaxies simulated at 'standard resolution' (250 $M_\odot$), while the bottom panels show high-resolution simulations (30 $M_\odot$). A length-scale of 10 kpc is shown in each of the top panels; the bottom panels are shown at the same scale.

below the detection limits (in surface brightness or stellar mass) of the observations used to calibrate the AM relations; moreover, the observations are of LG satellites, not isolated systems.

Extrapolations from fits at higher mass ($M_\star \gtrsim 10^9\,{\rm M}_\odot$) from Moster et al. (2013) and Behroozi, Wechsler & Conroy (2013) are also shown. Read et al. (2016b, 2017, not shown) argue for a power-law extrapolation from a relationship fit to isolated galaxies with $M_\star > 10^7\,{\rm M}_\odot$ and end up with a (slightly) higher normalization than even Behroozi et al. (2013) over the mass range studied here. These extrapolations fit to (much) higher mass are not tied to any local observations and have a wide range in estimated stellar masses for haloes in our mass range – one such extrapolation (Moster et al. 2013) lies immediately on top of our points while others (Behroozi et al. 2013; Read et al. 2016a, 2017) are much more shallow. Read et al. (2016b, 2017) calculate halo masses for 19 isolated dwarf irregular galaxies ($5 \times 10^5 \lesssim M_\star/{\rm M}_\odot \lesssim 10^8$) by a rotation curve fitting method developed by fitting model galaxies from idealized simulations. They show that the halo massed they derive match the extrapolated relation from isolated galaxies well. While we cannot fully explain the difference between our results and their halo mass estimates for these galaxies, it is interesting to note that because their simulations are idealized, they lack natural cosmological growth, as well as the expected suppression of SF in low-mass haloes at early times via a cosmic UV background. Furthermore, although our simulations are run without the presence of the MW, we must by necessity compare most of our galaxies (specifically the UFDs) to LG observations, and so it is heartening that our galaxies match the relations tuned to match the LG. For a more rigorous comparison of classical dwarf mass functions, see Garrison-Kimmel et al. (2018).

Our simulations suggest, at least absent a massive host such as the MW, UFDs form in all DM haloes with $M_{\rm vir}^{z=0} \gtrsim 5 \times 10^8\,{\rm M}_\odot$ (equivalently, $V_{\rm max}^{z=0} > 13\ {\rm km\,s^{-1}}$). This is just for galaxies with $\gtrsim$100 star particles: we form galaxies with at least 15 star particles in all haloes with $V_{\rm max}^{z=0} > 10\ {\rm km\,s^{-1}}$ and at least 1 star particle in all haloes with $V_{\rm max}^{z=0} > 7.5\ {\rm km\,s^{-1}}$. To get a (very crude) sense of the implications for LG dwarf populations, we can compare to the number of $V_{\rm infall} > 13\,{\rm km\,s^{-1}}$ haloes+subhaloes (where $V_{\rm infall}$ is $V_{\rm max}$ when the satellite crosses MW's virial radius) in DM-only simulations of 12 LG analogues from Garrison-Kimmel et al. (2014). This naively predicts ∼400–610 such MW satellites with $M_\star \gtrsim 10^3\,{\rm M}_\odot$, ∼180–380 'isolated' dwarfs above this mass in the Local Field[10] (within 1 Mpc), and up to 140 satellites of other field dwarfs in the same volume, where the range spans one standard deviation from the mean for the sample.

---

[10] The Local Field is the immediate environment of the MW and M31 outside of each massive galaxy's virial radii.

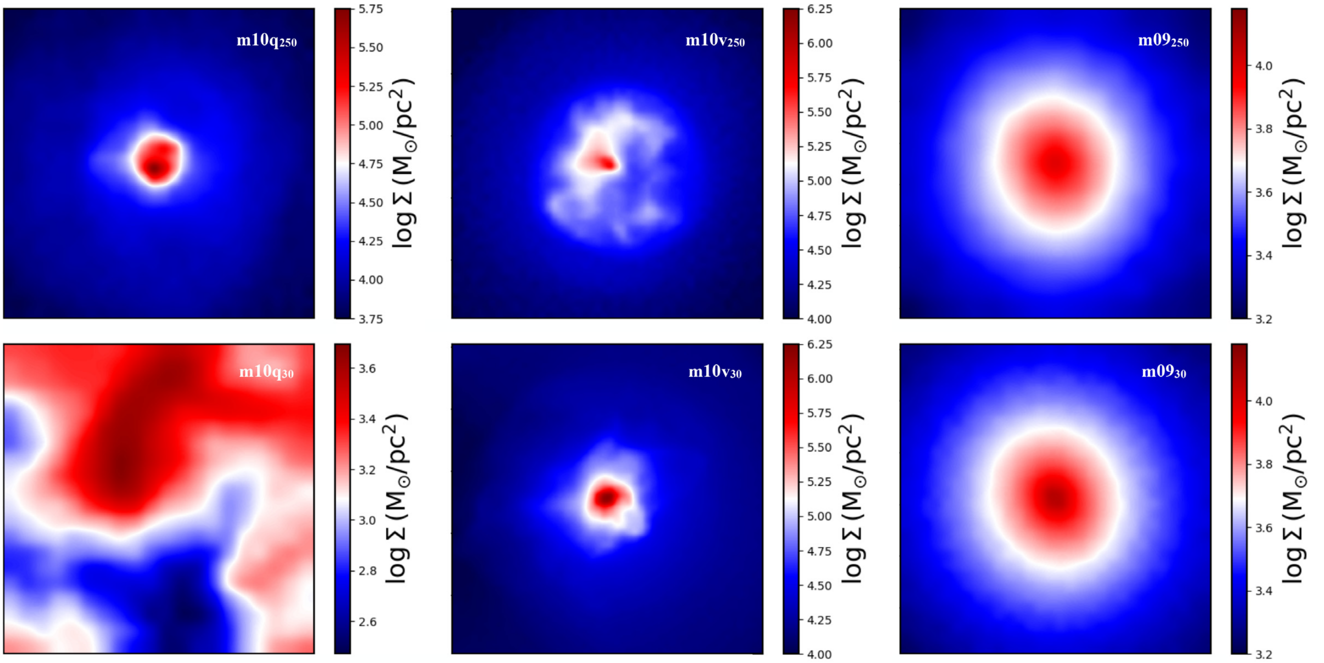

Figure 2. Gas surface density within the central 30 kpc for the same simulations shown in Fig. 1, and at the same physical scale. The low density of gas seen in m10q at the highest resolution (lower left panel) is related to its early quenching (see Section 3.2).

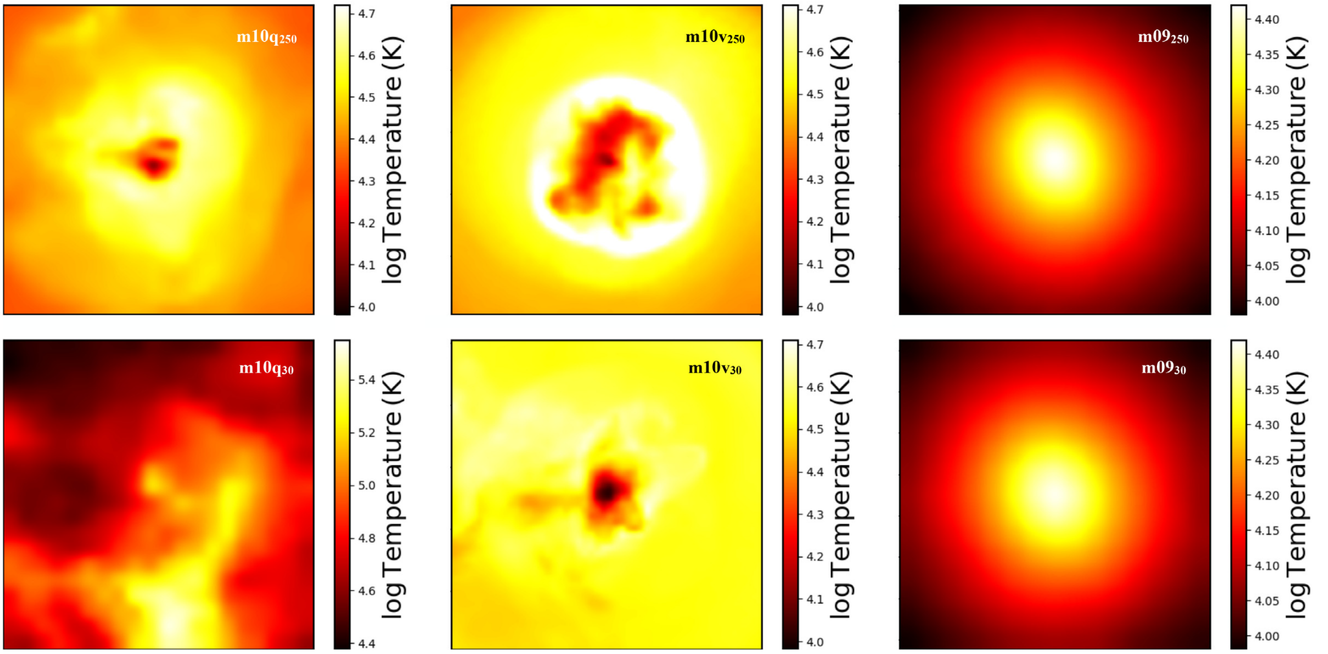

Figure 3. Gas temperature within the central 30 kpc for the same simulations shown in Fig. 1, and at the same physical scale. The high temperature of the gas seen in m10q at the highest resolution (lower left panel) is related to its early quenching (see Section 3.2).

However, the mere presence of a MW-mass galaxy at the centre of a halo has been shown to completely destroy ∼1/3–1/2 of all of its subhaloes (Garrison-Kimmel et al. 2017), so the number of satellites may be significantly less than these rough estimates. Using a higher $M_\star \gtrsim 10^4\ \mathrm{M}_\odot$ ($V_{\rm max} \gtrsim 20\ \mathrm{km\,s^{-1}}$) threshold gives results qualitatively consistent with the abundance-matching inferences for these populations in Dooley et al. (2017). Interestingly, the fact that we do not see a sharp cut-off in halo mass for UFDs is also consistent with the recent study by Graus et al. (2018), which argued the radial distribution of MW satellites requires haloes with $V_{\rm infall} \gtrsim 6{-}10\ \mathrm{km\,s^{-1}}$ be populated with UFDs. We will study the less well-resolved, but more abundant, lower mass UFD population in future work.

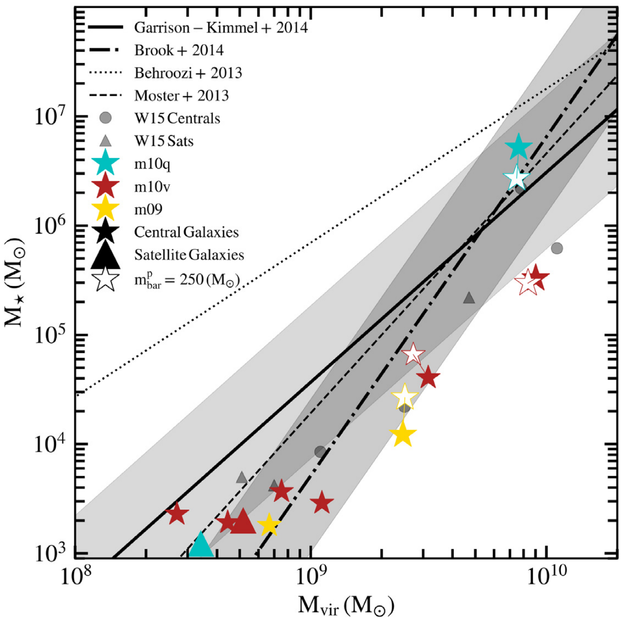

Figure 4. Stellar mass–halo mass ($M_\star$–$M_{\rm halo}$) relation for the resolved central galaxies (Table 1; filled/open symbols are the high/low resolution runs) compared to the abundance matching (AM) relations from Garrison-Kimmel et al. (2014) and Brook et al. (2014) with 0.7-dex scatter. We also show extrapolations from the AM relations of Moster, Naab & White (2013) and Behroozi et al. (2013) without the scatter. Both of these relations are extrapolated from fits to higher mass ($M_\star > 10^8\,{\rm M}_\odot$) galaxies, without fitting to lower mass observations. We stress that the comparison is purely heuristic/extrapolated: most of our simulated galaxies are well below detection limits for the observations used to calibrate the relations. Results from W15 are shown in grey.

3.2 Star formation histories

Figs 5–6 show the archaeological SFH for each galaxy (the distribution of formation times of all $z = 0$ stars), in cumulative and differential form. In every case, the more massive galaxies have SF down to $z < 0.5$, while all galaxies with $M_\star < 10^5\,{\rm M}_\odot$ had SF cease well before $z = 2$. The least massive UFDs, with $M_\star < 10^4\,{\rm M}_\odot$ in haloes with $M_{\rm halo} \lesssim 10^9\,{\rm M}_\odot$, have the most ancient populations, with SF ceasing before $z = 10$ (the mid-point of reionization, as modelled here).[11] This is consistent with the SFHs of LG dwarfs (Brown et al. 2014). Since our galaxies do not have a massive host, it is clear that the UFD quenching was driven by reionization, and not environmental effects. High-mass UFDs ($M_\star \sim 10^{4-5}\,{\rm M}_\odot$) have their accretion cut off by reionization at $z \sim 10$–6, but form stars for another ∼1 Gyr (until $z \sim 2$–4). This residual SF comes from gas that was accreted pre-reionization and is self-shielding to the UV background, so continues to form stars until it is exhausted or blown out by SNe (see also Oñorbe et al. 2015).

We note that the primary m10q galaxy appears to 'self-quench,' i.e. quench without external influence, and exhaust its cold gas before $z = 0$. This is also evident by the extremely low density and high temperature of the gas as seen in the lower left panel of Figs 2–3. Although this does not occur in the specific lower resolution run here (which has ongoing SF to $z = 0$), in several previous studies (see e.g. Su et al. 2018b) we have shown that this can occur somewhat stochastically, i.e. if a particularly large number of SNe explode concurrently, the burst can eject the remaining small amount of cold gas in the galaxy and shut down SF. Roughly, comparing iterations of m10q with intentionally small perturbations to the ICs or run-time parameters in Su et al. (2018b), Hopkins et al. (2018b) and the ensemble of dwarfs studied in Fitts et al. (2017), we find this occurs with order-unity probability. Without a statistical sample, we cannot say if it is more likely in high-resolution runs, but it does indicate that such gas expulsion is not purely an artefact of lower resolution. Whether this is consistent with observations requires a larger sample: Geha et al. (2012) argue the non-star-forming fraction in the field for galaxies with $10^7\,{\rm M}_\odot < {\rm M}_\star < 10^9\,{\rm M}_\odot$ is zero, but several obviously quenched counter-examples with $M_\star \lesssim 10^7\,{\rm M}_\odot$ exist out to >1 Mpc from the LG (Karachentsev et al. 2001, 2014, 2015; Makarov et al. 2012; Cole et al. 2014; Makarova et al. 2017), and Fillingham et al. (2018) argue that the quenched fraction in the LG and field dwarfs requires some internal quenching (i.e. unconnected to a massive host) must occur at these masses.

Fig. 6 shows the star formation rate (SFR) averaged in 10 and 200 Myr windows, analogous to time-scales over which H α and UV continuum measurements are sensitive; we find the SFRs are bursty, as found previously at lower resolution (Muratov et al. 2015; Sparre et al. 2017; Faucher-Giguère 2018). SFRs for the other simulated UFDs are similar to m09$_{30}$ shown. The results are qualitatively similar at low/high resolution, although the periods of low SFR in the low-resolution runs drop to zero while remaining finite at high resolution – this is simply an artefact of the discrete nature of our star particles (at $\dot{M}_* \sim 10^{-6}\,{\rm M}_\odot\,{\rm yr}^{-1}$, it requires ∼250 Myr to form a single star particle at ∼250 ${\rm M}_\odot$ resolution). Quantitatively, whether the burstiness changes with resolution depends on our definition. The unit of SF (a star particle) is larger at low resolution, so sampling variations decrease at higher resolution. Based on the metric used in Hopkins et al. (2014), namely the dispersion in $\log(\langle \dot{M}_*(\Delta t_1)\rangle / \langle \dot{M}_*(\Delta t_0)\rangle)$ (where $\Delta t_1 \sim 10$ Myr and $\Delta t_0 \sim$ Gyr), we actually find the burstiness slightly *increases* in higher resolution runs. However, quantifying burstiness in terms of the fraction of the total M_* formed in periods where $\langle \dot{M}_*(\Delta t_1)\rangle > 1.5\,\langle \dot{M}_*(\Delta t_0)\rangle$ (Sparre et al. 2017), we find slightly decreasing burstiness at higher resolution (for $\Delta t_1 \sim 10$ Myr; for much longer averaging times, the effect vanishes). In all cases, the resolution dependence is small (∼10 per cent for order-of-magnitude change in resolution).

3.3 Cusps and cores

Fig. 7 shows the DM profiles of the primary galaxies versus resolution. It is well known that convergence in the halo mass profiles of *N*-body calculations is almost entirely determined by mass resolution (see e.g. Power et al. 2003), so the simulations here provide an important convergence test. Using the most conservative definition of a converged radius from Power et al. (2003), our ultra-high resolution DM profiles should be converged down to ∼60–100 pc; using the more-aggressive criterion from Hopkins et al. (2018b) gives ∼30–40 pc. Inside of this Power radius, profiles will tend to flatten for numerical reasons.

However, episodes of strongly clustered SF that cycle between dense GMCs and explosive outflow can produce physical cored DM profiles (Pontzen & Governato 2012; Di Cintio et al. 2014b; Chan et al. 2015; Oñorbe et al. 2015). Hopkins et al. (2018b) considered a 'full physics' resolution study of the DM profiles in m10v and m10q here at lower resolution (from 250 to $10^5\,{\rm M}_\odot$), and argued that convergence was dominated by the baryonic effects, not traditional *N*-body considerations, especially in the more massive m10q. We

---

[11] The one exception appears to be a single star particle from m10v$_{30}$ Sat, likely a contaminant from its host m10v$_{30}$.

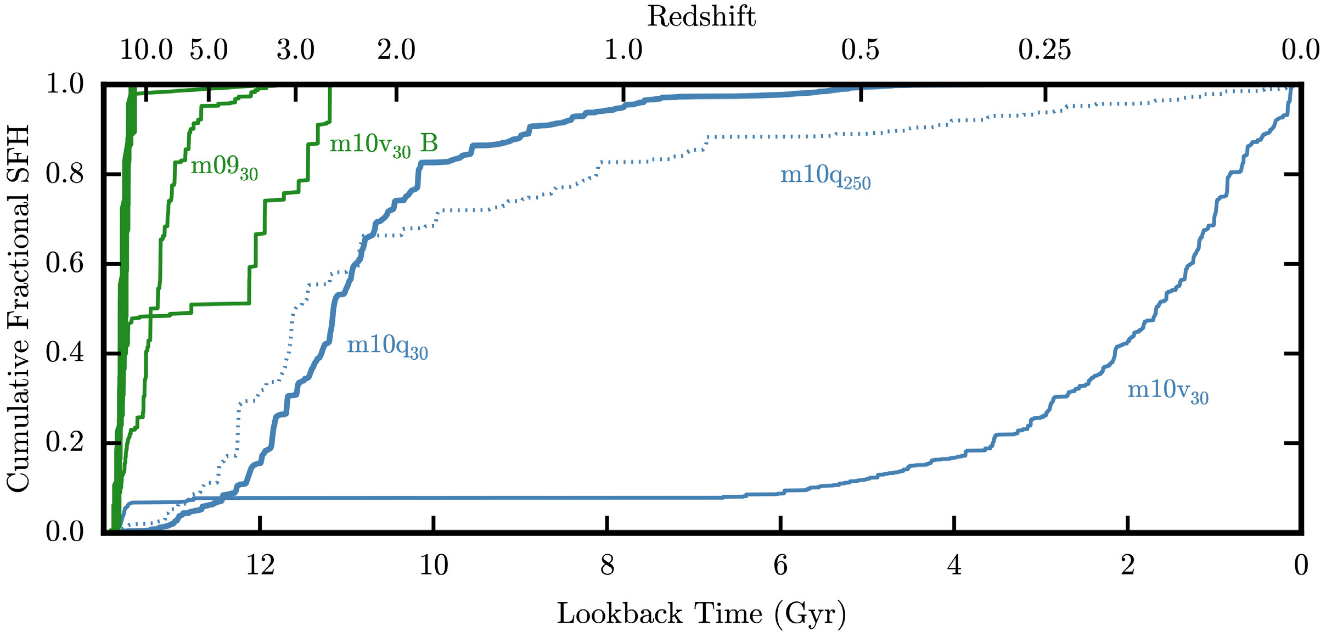

Figure 5. SFHs for each high-resolution galaxy in Table 1. Colours distinguish classical dwarfs ($M_\star > 10^5\,\mathrm{M}_\odot$; *blue*) and UFDs ($M_\star < 10^5\,\mathrm{M}_\odot$; *green*). Every classical dwarf analogue formed in our simulations has SF until $z < 0.5$, while all UFDs have had their SF shut down before $z = 2$. Because these are isolated UFDs, this suggests that reionization quenched these objects. The dotted line shows m10q$_{30}$ at lower resolution. Its higher resolution counterpart (upper blue line) does not show the same trickle of SF at $z = 0$–0.5, but this appears to be stochastic: re-running the low-resolution version with slightly perturbed initial conditions, we find its SF continues or peters out with approximately equal likelihood.

confirm this here: at higher resolution, the core in m10q is *more* pronounced, exactly as expected given its *larger* stellar mass in that particular run. Given the weak dependence of burstiness on resolution, it is not surprising that the cusp/core behaviour also remains robust.

Most importantly, as predicted by the much lower resolution simulations referenced above, *all* our UFDs (which all have $M_\star/M_{\rm vir} < 10^{-4}$), including those not shown, exhibit cusps down to at least 50–100 pc. For those UFDs that exhibit ∼100 pc cores, the deviation from a Navarro-Frenk-White (NFW) profile occurs just outside of the converged radius, and is likely in part due to imperfect centring on the dark matter. Furthermore, the half-light radii of the UFDs are all substantially larger than their numerical convergence radii, further indicating that measurable dynamics of such UFDs (which are sensitive to the total mass within the deprojected half-light radius; see below and Wolf et al. 2010) would point to dark matter cusps. However, it is important to note that the lack of cores predicted in UFDs is resolution limited, and allows for the presence of small $\lesssim$100 pc cores to be detected observationally without posing a challenge to the model.

3.4 Kinematics and galactic structure

3.4.1 Sizes and surface brightness distributions

Our result that every isolated dark matter halo with $M_{\rm vir} > 4.4 \times 10^8\,\mathrm{M}_\odot$ forms a UFD suggests that these objects may be ubiquitous in the field. However, these low-mass haloes have shallow potential gravitational wells, causing the galaxies that form within them to have larger effective radii and extremely low surface brightnesses (Kaufmann, Wheeler & Bullock 2007; Bullock et al. 2010; Bovill & Ricotti 2011a, b; W15). This means that, despite their abundance, they may be very difficult to detect. W15 calculated values for $R_{1/2}$, the 2D projected half-mass radius, for their lowest mass UFDs ($M_\star \lesssim 10^4\,\mathrm{M}_\odot$) that lied in the range 200–500 pc, making them undetectable with current surveys such as the Sloan Digital Sky Survey (SDSS; York et al. 2000). However, because the galaxies studied had only tens of star particles, and the size of galaxies is highly sensitive to resolution, there was a possibility that the $R_{1/2}$ of the UFDs was not resolved.

The left-hand panel of Fig. 8 shows the mass–size relation for our much better resolved dwarfs alongside data for classical MW dwarfs (McConnachie 2012, open black circles), year 1 and 2 UFD candidates galaxies from the Dark Energy Survey (DES; Bechtol et al. 2015; Drlica-Wagner et al. 2015), Hydra II (Martin et al. 2015), Virgo I (Homma et al. 2016), and Cetus III (Homma et al. 2018) for the last two galaxies, we used their stellar mass estimates under the assumption of a Kroupa IMF (Homma et al. 2018 give several estimates depending on the assumed IMF) in order to be consistent with the simulations, which use the same IMF. Also shown in the figure is a surface brightness detection limit of $\mu_{\rm V} = 30$ mag arcsec^{-2} for solar absolute magnitude $\mathrm{M}_{\odot,\,V} = 4.83$ assuming a stellar mass-to-light ratio of $M_\star/L \approx 1\,\mathrm{M}_\odot/\mathrm{L}_\odot$ (so this corresponds to a physical, bolometric $0.036\,\mathrm{L}_\odot\,\mathrm{pc}^{-2}$). For example, a Plummer profile with central surface brightness $\Sigma_{\rm peak} = L/\pi\, R_{1/2}^2$, this corresponds to the surface brightness detection limit for SDSS. We also compare the improved limit 32.5 mag arcsec^{-2} which is anticipated for upcoming surveys such as the co-added Large Synoptic Survey Telescope (LSST).

Our more massive galaxies agree well with observed systems in Fig. 8, while the lowest mass UFDs have even lower surface brightnesses than those of W15 in the same mass range. Every UFD with $M_\star < 10^4\,\mathrm{M}_\odot$ in our sample has $R_{1/2} > 400$ pc, lying close to or above the likely LSST detection limit, which suggests that they may well go undetected for some time. The sizes of these are much larger than our force softening or the mass-resolution-based

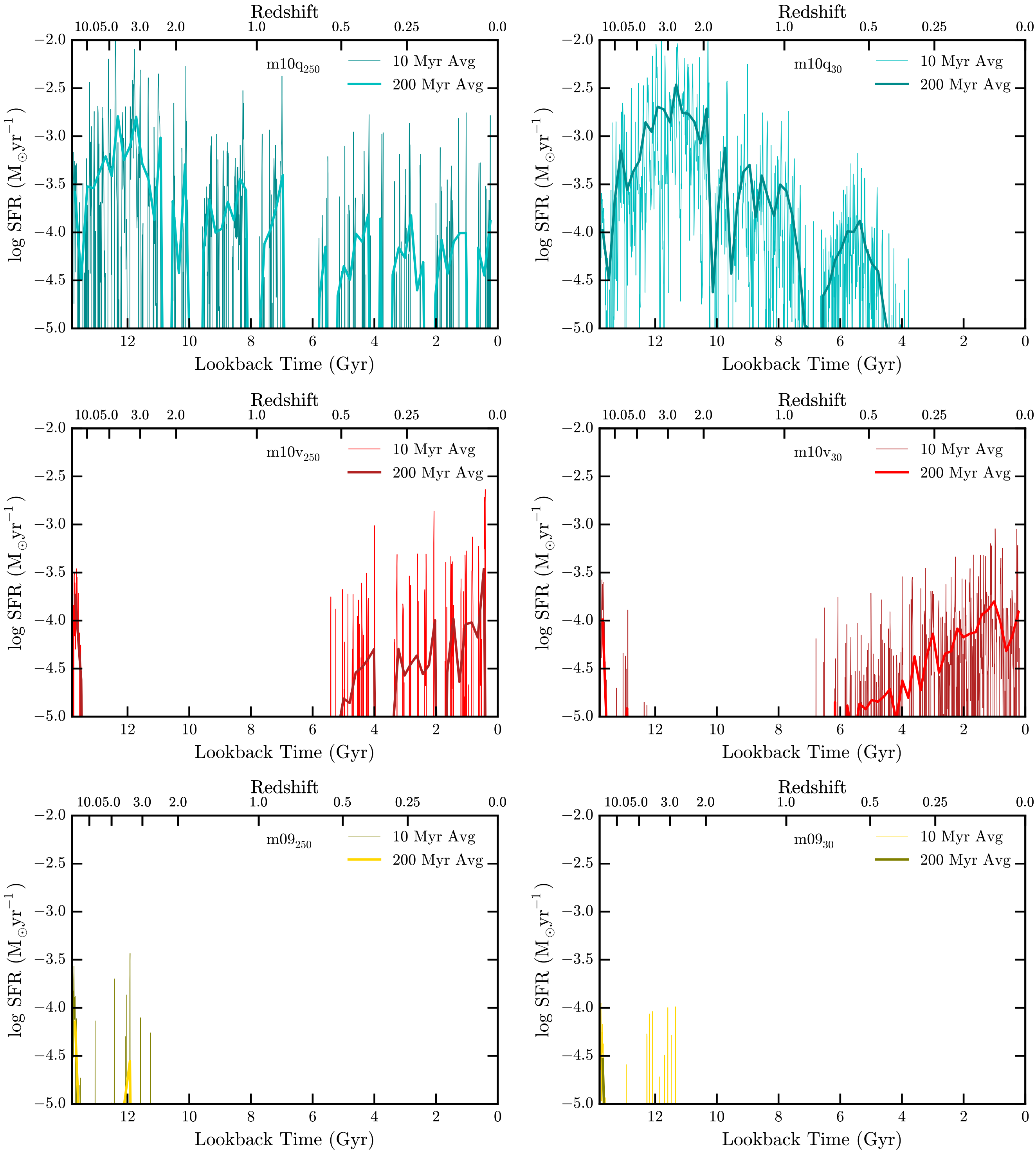

Figure 6. Star formation rate (SFR) versus time for the three 'primary' galaxies resolved in both our lower (250 M$_\odot$; *left*) and higher (30 M$_\odot$; *right*) resolution boxes. The thin (thick) lines are averaged in 10 Myr (200 Myr) intervals. At higher resolution, the gaps where the SFR drops to approximately zero are (at least partially) filled in, although all of the galaxies exhibit considerable burstiness in their SFHs.

Power et al. (2003) convergence radius discussed above (< 30 pc), so this is likely robust. Moreover, where we do see (small) changes in size with resolution, the galaxies essentially move along close-to-constant surface brightness tracks.

Interestingly, there does not seem to be any tight correlation in the simulated galaxies between $R_{1/2}$ and $M_\star$, at $M_* \ll 10^7$ M$_\odot$. This is yet another indication that galaxy formation prescriptions with simplistic recipes for determining galaxy size, or the assumption that $R_{1/2} \propto r_{\rm vir}$ (as in e.g. Mo, Mao & White 1998; Kravtsov 2013), fail for the lowest mass galaxies (see also Kaufmann et al. 2007). The recent detection of ultra-diffuse galaxies (UDGs) likewise suggests that even more massive dwarfs have wildly varying effective radii

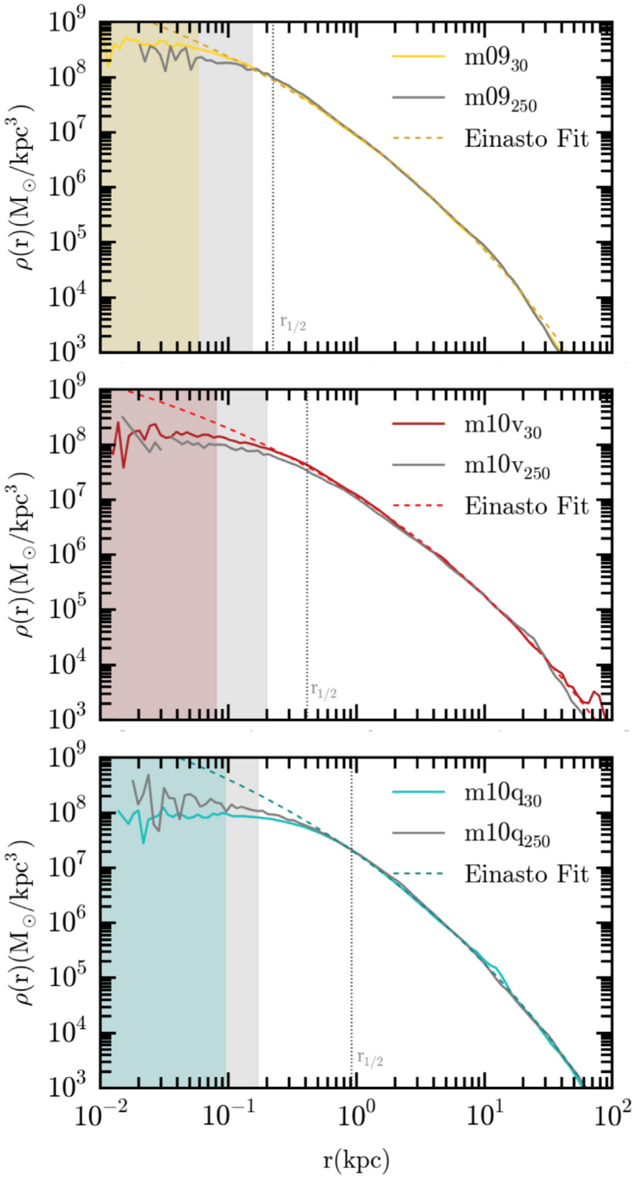

Figure 7. DM density as a function of radius for the three 'primary' galaxies from Table 1. Results from both standard (grey) and high-resolution (coloured) simulations are plotted along with an Einasto profile that was fit to the $m^{\rm p}_{\rm bar} = 30$ runs over the range $0.01 < r/r_{\rm vir} < 1$. The shaded ranges show the regions enclosing $<$2000 DM particles (coloured the same way as the line of the corresponding run). The 3D half-stellar-mass radius is shown as a vertical dotted line. The resolution differences are small and do not change the cusp/core distinction. Moreover, the differences are not dominated by dynamical or *N*-body convergence but rather by the differences in the SFHs: runs where the central DM density is slightly higher/lower corresponds to runs which produces slightly fewer/more stars (hence less/more SNe energy). Although some numerically resolved weak cores are present at $\lesssim$50–100 pc, cores with a truly flat log-slope extending to $\gtrsim$300 pc only appear when $M_\star/M_{\rm vir} \gtrsim 10^{-4}$ (only m10q here).

(several dex range) for galaxies at a single M_* (van Dokkum et al. 2015). The *apparent* size–mass relation in the observations (Fig. 8) is clearly an effect of the surface brightness limit (where most of the galaxies pile up, as noted by the authors of the survey studies cited above). Crucially, it is likely that *most* UFDs lie at lower surface brightness (larger radii at fixed stellar mass) than we currently can detect. The discovery of a new MW satellite in the *Gaia* Data Release 2 with $\mu_{\rm V} = 32.3$ mag arcsec^{-2} – 100 times more diffuse than most UDGs – is likely the first indication of what is to come in the extremely low surface brightness sky (Torrealba et al. 2018).

It is noteworthy that our simulations do not reproduce those UFDs with half-light radii in the 100 pc, given how well they agree with many other properties of observed dwarfs. To check whether this is also a selection effect, we restrict those dwarfs in our sample that have average surface brightnesses $>$ 30 mag arcsec^{-2} to an annulus that encloses only the central region of the galaxy with at least that surface brightness. Doing so reduces both $R_{1/2}$ as well as $M_\star$, which yields $R_{1/2} \sim 100$ pc ($R_{1/2} < 200$ pc) and $M_\star = 3.6 \times 10^3$ M$_\odot$ ($M_\star = 2.7 \times 10^4$ M$_\odot$) for m09$_{30}$ (m10$_{30}$ B) – bringing both into the region occupied by the DES UFDs. This suggests that observations may only be sensitive to the 'bright' core of more massive objects and raises an intriguing question: do the DES UFDs all have diffuse (and relatively massive) outer haloes that are currently invisible to us?

3.4.2 *Dynamical masses and sizes*

Although our lowest mass simulated galaxies show no overlap with observations in the stellar mass–size plane, there *is* significant overlap with observations in the dynamical mass–size plane. The right-hand panel of Fig. 8 shows $R_{1/2}$ versus $M_{1/2}$, where $M_{1/2} \simeq 4\,\langle\sigma^2_{\rm los}\rangle\, R_{1/2}/G$ $M_{1/2}$ is an estimate of the total (dynamical) mass from $\sigma_{\rm los}$, the line-of-sight stellar velocity dispersion (see e.g. Wolf et al. 2010). We compare observed systems from Collins et al. (2013) with $R_{1/2}$ taken from Kirby et al. (2014) where available, and McConnachie (2012) otherwise. The simulations agree well with the data at the radii/masses both sample (see also Campbell et al. 2017; González-Samaniego et al. 2017; Errani, Peñarrubia & Walker 2018), and with the true mass within the 3D half-stellar-mass radius (endpoints of coloured bars).

The overlap between all simulated and observed galaxies in the right-hand panel of Fig. 8 means that the very diffuse galaxies in the left-hand panel, which would be invisible to current observational surveys, do not inhabit dark haloes that are fundamentally different from those hosting analogues of observed systems. The truly remarkable aspect of these galaxies is their large half-light radii; the underlying mass distributions, which are strongly dominated by dark matter at all radii, look just like standard predictions of CDM. For $r \ll r_{\rm s}$, where $r_{\rm s}$ is the NFW scale radius, we expect that $M_{\rm enclosed}(< r) \propto r^2$; this is precisely the correlation seen in Fig. 8.

3.4.3 *Rotation*

Observations of both dSphs and dIrrs in the Local Volume suggest that most dwarf galaxies have kinematics dominated by random motions (Wheeler et al. 2017, hereafter W17). This can be seen in Fig. 9 for an observational sample of 30 dSphs and dwarf ellipticals and 10 isolated dwarfs in the LG taken from W17. Following their prescription to calculate $v_{\rm rot}/\sigma$ for our simulations, where $v_{\rm rot}$ is the rotation across its axis and σ is the underlying (constant) line-of-sight velocity dispersion, we perform a Bayesian analysis on the positions and velocities of each simulated galaxy along independent lines of sight. We explore two models for $v_{\rm rot}$: a flat model that assumes constant rotation, $v_{\rm rot}(R) = v_{\rm o}$, and a radially varying pseudo-isothermal sphere, $v_{\rm rot} = v_{\rm o}\sqrt{1 - R_{\rm o}/R\,\arctan(R/R_{\rm o})}$, where R is the distance from the rotation axis on the plane of the sky and $v_{\rm o}$

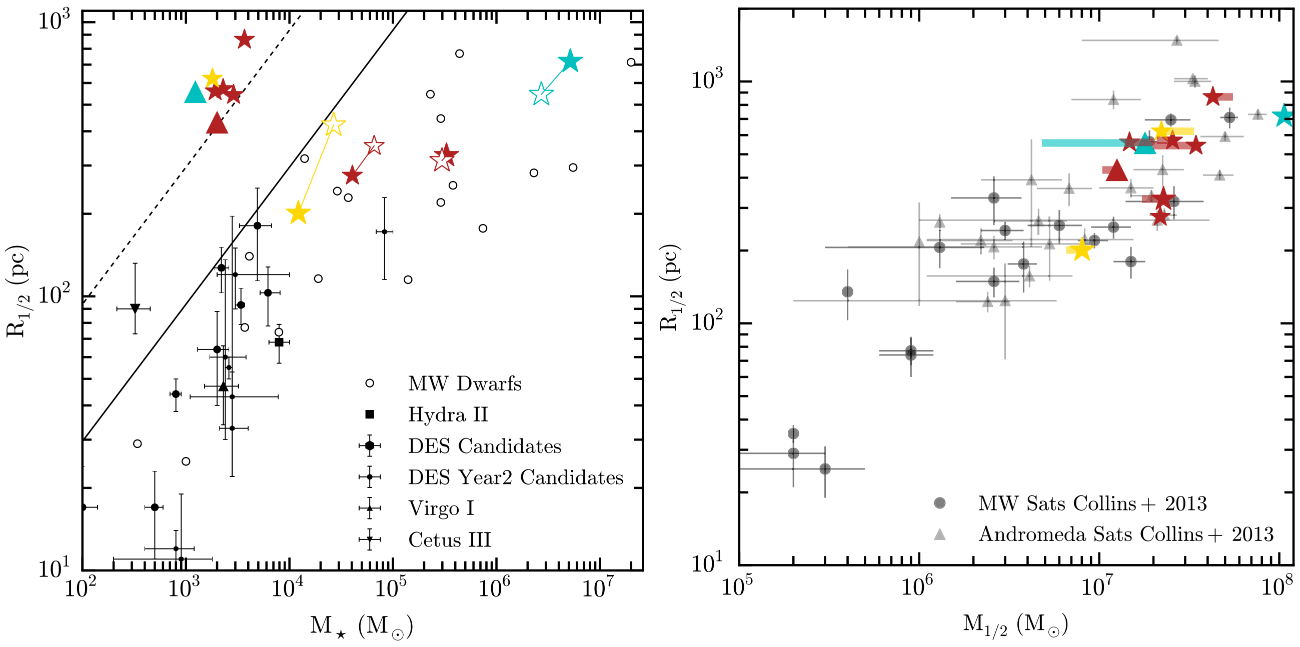

Figure 8. *Left*: 2D half-stellar-mass radii ($R_{1/2}$) versus $M_\star$ for galaxies in Table 1 (symbols for the simulations as Fig. 4). We compare our results with observed MW dwarfs compiled from (McConnachie 2012), DES candidates (Bechtol et al. 2015), (Martin et al. 2015), Virgo I (Homma et al. 2016), and Cetus III (Homma et al. 2018). The solid line is a typical surface brightness limit of these surveys, 30 mag arcsec^{-2} (for $M/L \approx M_\odot/L_\odot$). Most of our UFDs will only be visible with future surveys (the dashed line shows a surface brightness limit of 32 mag arcsec^{-2}). *Right:* dynamical mass $M_{\rm half}$ computed using the Wolf et al. (2010) formula (as is done with observations) versus $R_{1/2}$; a wide coloured bar extends from the estimated value to the true dynamical mass inside the 3D half-stellar-mass radius. We also show measured values for MW+Andromeda satellites ($M_{1/2}$ from Collins et al. 2013, $R_{1/2}$ from Kirby et al. 2014 and McConnachie 2012). The agreement in sizes and stellar+dynamical masses is excellent (where observable), except for m10q$_{30}$ Sat, which likely suffers from contamination from its host.

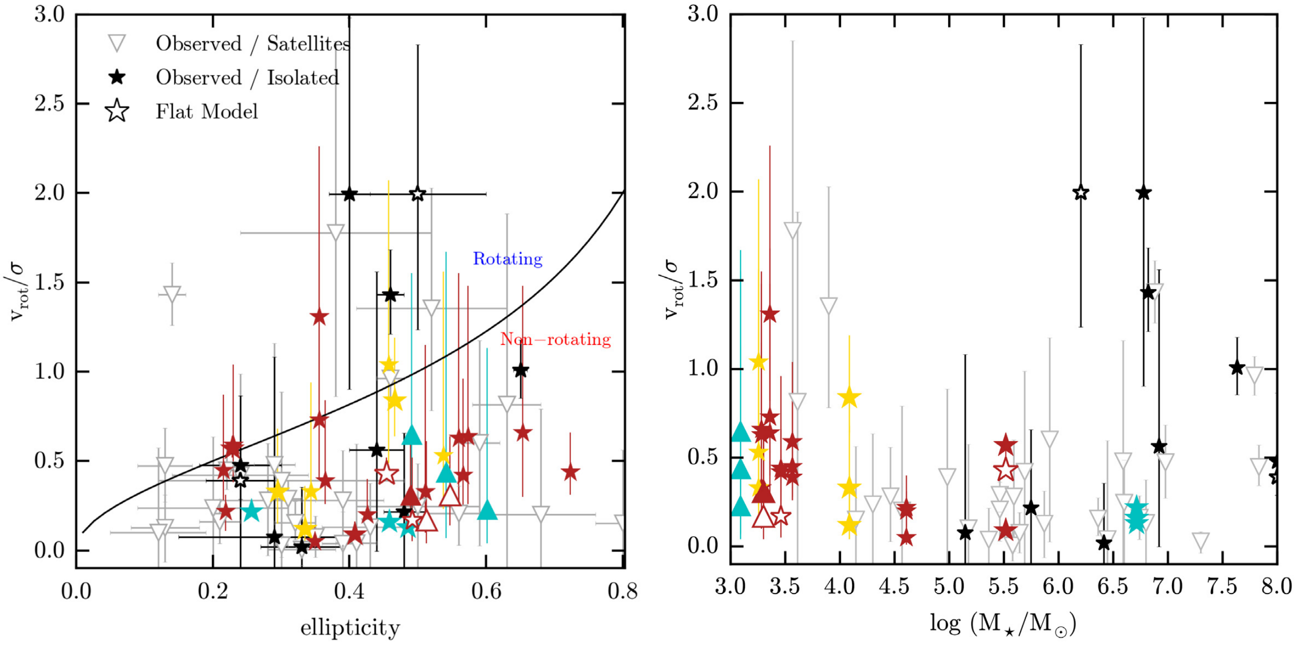

Figure 9. *Left*: stellar rotation support $v_{\rm rot}/\sigma$ versus ellipticity for observed isolated LG dwarfs (compiled in Wheeler et al. 2017) and our simulations; the distributions are very similar. The open symbols for the simulations and the isolated observations prefer a flat rotation model. None of the observed satellites prefer a flat model. The solid line shows the expectation for self-gravitating systems flattened entirely by rotation (as opposed to anisotropy; Binney 1978); most UFDs (field or satellite) are not rotation dominated. *Right:* $v_{\rm rot}/\sigma$ versus stellar mass. The distributions are again very similar where they overlap in mass. At high mass ($>10^6\,M_\odot$), we only have one galaxy (m10q, which has low but significantly non-zero $v_{\rm rot}/\sigma$), so more statistics are needed.

and $R_{\rm o}$ are the rotation velocity and rotation radial scale parameters, respectively (see W17 for details).

Fig. 9 shows $v_{\rm rot}/\sigma$ versus ellipticity for all simulations (with three independent viewing angles for each), as well as data from W17. The solid line is the locus occupied by oblate isotropic rotators (galaxies flattened primarily by rotation; see Binney 1978). Objects below the line are generally understood to be pressure supported. Seven of the 10 isolated dwarfs (black stars) show no clear signs of rotation; the same is true for nearly all of the LG satellites (grey downward triangles). In addition to posterior probabilities for $v_{\rm rot}$ and σ, the model calculates the Bayesian evidence for both rotation versus non-rotation and flat model versus radially varying models. Objects that prefer a flat model are shown as open symbols for the isolated observed dwarfs and the simulations. None of the observed satellites prefer a flat model. Fig. 9 also shows $v_{\rm rot}/\sigma$ versus M_*.

Our simulated galaxies show a remarkably good overlap with the observed data in both of these planes. With higher resolution and the newer FIRE-2 code, we find marginally more rotation than the FIRE-1 simulations from W17, but the difference is small. Although all three of the more massive dwarfs do have Bayesian evidence for rotation, none have high $v_{\rm rot}/\sigma$. At high masses ($\gtrsim 10^6\,{\rm M}_\odot$), our sample has just one galaxy (m10q) that has low $v_{\rm rot}/\sigma$. Since most observed systems are also non-rotating at this mass, this is expected, but large $v_{\rm rot}/\sigma \sim 2$ begins to appear at these masses; it therefore would be interesting to explore this mass regime with better statistics.

3.5 Chemical abundances

Kirby et al. (2013a) used stellar metallicities to demonstrate that the relationship between stellar mass and stellar metallicity extends, unbroken, down to MW and M31 dwarf spheroidals, irregulars, and even UFDs down to $M_\star \sim 10^{3.5}\,{\rm M}_\odot$. This is a striking result, as the sample includes both satellites and isolated dwarfs, meaning the relationship is unaffected by infall into a more massive host. Fig. 10 explores the extremely low-mass end of the (stellar) mass–(stellar) metallicity relation (MZR), comparing observations from Kirby et al. (2013a) and Vargas, Geha & Tollerud (2014) for MW+Andromeda satellites. There is an obvious and intriguing discrepancy between observed and simulated galaxies, which increases to nearly 2 dex towards lower masses.

We emphasize that at higher masses ($\gtrsim 10^9\,{\rm M}_\odot$) previous studies with the same FIRE physics have extensively compared stellar and gas-phase MZRs at both $z = 0$ and higher redshifts and found remarkably good agreement between observations and simulations in [Fe/H] as well as other species ([O/H], [Mg/H], [Z/H], etc.; see Wetzel et al. 2016; El-Badry et al. 2017; Ma et al. 2017a, b; Escala et al. 2018; Hopkins et al. 2018b). The discrepancy reported here appears to be specific to low-mass dwarfs. We also emphasize that the discrepancy is not unique to [Fe/H], as [Mg/H] and other species show a similar (albeit slightly weaker) offset, nor to the method by which [Fe/H] is weighted (e.g. light-or-mass weighting or taking $\langle[{\rm Fe/H}]\rangle$ versus $[\langle{\rm Fe}\rangle/\langle{\rm H}\rangle]$ give a qualitatively similar result).

What could cause this? Recall, our simulations adopt a very simple IMF-sampling and yield model: even though SNe are discrete, the yields are IMF averaged, and most yields are independent of the progenitor metallicity (see Hopkins et al. 2018b for details); they therefore reflect yields at solar metallicity, where they are best understood both theoretically and observationally. Yield predictions for extremely metal-poor stars in the literature differ by as much as ∼1 dex (Woosley & Weaver 1995; François et al. 2004), so a strong dependence on progenitor metallicity could explain the offset seen here. It is also possible that the discrepancy has its origin in differential re-incorporation of metals (versus ejection in galactic winds): our dwarfs *produce* sufficient metals to lie on the MZR, if they retained them all and re-incorporated them into new stars in a closed-box fashion. But this is difficult to reconcile with the strong outflows required to explain their very low stellar masses (Kirby, Martin & Finlator 2011).

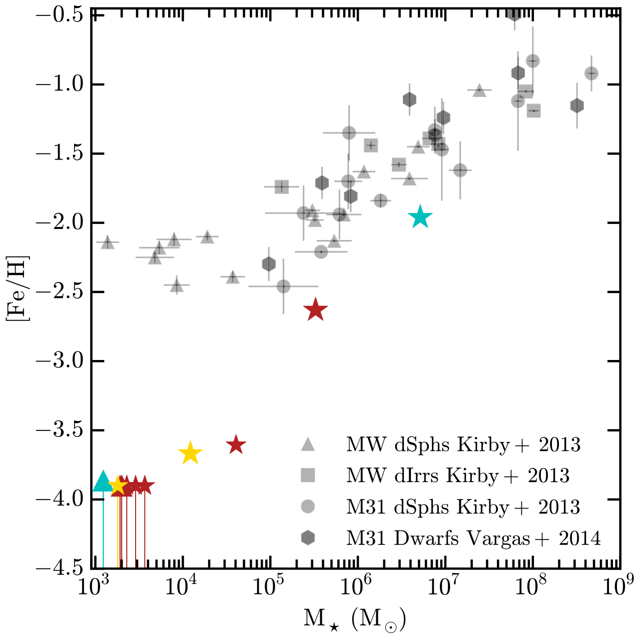

Figure 10. Stellar mass ($M_\star$) versus metallicity ([Fe/H]) for LG dwarfs (Kirby et al. 2013a, grey points) and our simulations (coloured symbols). The simulated UFDs at [Fe/H] ∼ −4 are at the baseline initial metallicity of the simulation (hence arrows indicating upper limits). While more massive ($\gg 10^7\,{\rm M}_\odot$) galaxies agree very well with the observed mass–metallicity relation (see Ma et al. 2017a, b; Escala et al. 2018), below $\sim 10^7\,{\rm M}_\odot$ the simulations begin to predict lower [Fe/H], with the discrepancy increasing towards lower masses. This may indicate satellites in the LG were pre-enriched by the (much more massive) MW+Andromeda, or by Pop-III stars (not included here; see the text for discussion).

Perhaps more importantly, our simulations include no explicit model for hyper metal-poor or metal-free Population-III stars (this is the reason why they are initialized with a metallicity ‘floor’ of [Fe/H] = −4).[12] Theoretical calculations suggest a *single* massive Pop-III star exploding in a pair-instability SN could produce $\gtrsim 100\,{\rm M}_\odot$ in heavy elements (Kozyreva, Yoon & Langer 2014) – sufficient to enrich $\gtrsim 3\times10^6\,{\rm M}_\odot$ worth of gas (comparable to the mass of our *most massive* galaxy studied here) to the minimum metallicity [Fe/H] ∼ −2.5 observed. Indeed, a number of recent studies have argued that an early Pop-III phase should pre-enrich almost all star-forming galaxies in haloes more massive than $10^8\,{\rm M}_\odot$ to [Fe/H] ∼ −2, even by $z \gtrsim 15$ (Chen 2015; Jaacks et al. 2018). Since these would leave no other relics, they would

---

[12] We note that halo m10v$_{30}$ was run with [Fe/H] = −5, and so we illustrate this by moving the points at the floor in that run up to the higher floor in the other runs and drawing lines to indicate that these are upper limits – the points would lie at whatever floor we initiate in the simulations. Because we do not explicitly model the transition between Population III and Population II stars, all low-metallicity ([Fe/H] < −2) SF is essentially identical, with metallicity acting as a tracer at the halo masses modelled here.

not change our other predictions, but presumably they would leave unique, testable abundance patterns in the observed dwarfs.

Another interesting possibility is that pre-enrichment occurs not via Pop-III stars but environmentally (from the more massive MW/Andromeda host), as the observed dwarfs are all LG satellites. Given typical progenitor masses of MW+Andromeda-mass systems at $z \gtrsim 6$, if just ∼1 per cent of the metals produced by SNe at these times escapes to ∼100 kpc physical radii, then a ∼1 Mpc co-moving volume would be polluted to $[\mathrm{Fe/H}] \sim -2$. To test this, we consider the simulations (using the identical code and physics) of LG-mass, MW+Andromeda-like pairs, presented in Garrison-Kimmel et al. (2018). While the resolution of these simulations (∼3000 $\mathrm{M}_{\odot}$) is extremely high for such massive haloes, it is not sufficient to resolve the lowest mass UFDs. However, we can directly compare [Fe/H] values for galaxies at $M_{\star} > 10^5\,\mathrm{M}_{\odot}$. We find that there is still a 0.5–1 dex offset between the simulated satellite galaxies within 300 kpc of the Galactic Centre and the observations, suggesting that pre-enrichment from a massive neighbour is not enough to relieve the discrepancy for massive dwarfs.

To get a sense for how the presence of a host galaxy may affect lower mass satellites, we consider that all of the galaxies with $M_{\star} < 10^5\,\mathrm{M}_{\odot}$ from Kirby et al. (2013b) are within 150 kpc of the Galactic Centre. If we measure the [Fe/H] values for the gas enclosed within the radius occupied by 90 per cent of those stars traced back to higher redshift, while excluding the inner 10 per cent to eliminate the galactic disc, we determine that ∼20 per cent (1 per cent) of the gas has been enriched to $[\mathrm{Fe/H}] \sim -2.5$ by $z = 4$ ($z = 10$). This means that, for the more massive UFDs that are still forming stars to $z \sim 2$, pre-enrichment from nearby massive host could explain the discrepancy. Additionally, preliminary examination of an extremely high resolution (∼900 $\mathrm{M}_{\odot}$) version of the MW-mass halo studied in Wetzel et al. (2016), run to $z \sim 4$, shows several satellites pre-enriched to $[\mathrm{Fe/H}] \sim -2.5$ by $z = 5$. However, for the lowest mass UFDs that have completed SF by $z = 10$, this mechanism alone is insufficient to explain the discrepancy.

4 COMPARISON TO PREVIOUS WORK

4.1 FIRE simulations

W15, Oñorbe et al. (2015, hereafter O15), and W17 investigate a similar set of simulations, all run with FIRE-1 physics, and with $m^{\mathrm{p}}_{\mathrm{DM}} \sim 1.3{-}2.5 \times 10^3\,\mathrm{M}_{\odot}$, $m^{\mathrm{p}}_{\mathrm{bar}} = 255\,\mathrm{M}_{\odot}$, $\mathrm{DM}_{\mathrm{soft}} = 25{-}35$ pc, and $\mathrm{g}_{\mathrm{soft}} \sim 1{-}2$ pc. Only W15 and W17 study the ultra-faint satellites of the more massive dwarfs, and include two additional simulations not presented in O15. Because their resolution is an order of magnitude lower than the highest resolution simulations we present here, the UFDs in W15 and W17 are resolved with only tens of star particles, and yet their results are broadly consistent with the results presented here. In addition to matching the stellar masses within a factor of approximately three, the SFHs in all three works show the same dichotomy between UFDs and more massive dwarfs that we find here.

O15 find that a large (∼1 kpc) core can form in certain $M_{\mathrm{halo}} \sim 10^{10}\,\mathrm{M}_{\odot}$ dwarfs if SF occurs mostly at late times. However, the feedback deposit scheme used in FIRE-2 is more similar to the prescription used in their earliest forming run of the same dwarf.[13] That dwarf only forms a ∼400 pc core. The sensitivity of their results to mild changes in the feedback implementation supports the idea that $10^{10}\,\mathrm{M}_{\odot}$ haloes lie at a transition mass, above which significant core formation starts to occur (Chan et al. 2015).

Interestingly, UFDs in W15 all have 30 mag arcsec$^{-2} \lesssim \mu_{\mathrm{V}} \lesssim$ 32.5 mag arcsec^{-2}, placing them within potential reach of current surveys such as DES and PanSTAARS, and certainly within reach of LSST. In this updated work, with an order of magnitude better resolution, our UFDs have *larger* $R_{1/2}$ values. This suggests that our results may be insensitive to numerical heating, as we would expect higher resolution UFDs to have smaller $R_{1/2}$ values if artificial expansion were occurring.

O15 investigate the MZR for their dwarfs, of which only one is a UFD, and find much better agreement with observations than found in this work. However, in all FIRE papers written before Escala et al. (2018), [Fe/H] was calculated by first averaging the abundances, and then taking the log to obtain [Fe/H]. This method is better for comparing to diffuse stellar populations in distant galaxies rather than to a collection of resolved stars, as is done in dwarfs. It leads to overestimating [Fe/H] and serves to mask the discrepancy between the results calculated in this way and observations in low-mass galaxies.

Fitts et al. (2017, hereafter F17) use the updated FIRE-2 code to run a much larger set of $M_{\mathrm{halo}} \sim 10^{10}\,\mathrm{M}_{\odot}$ dwarfs than W15 or O15, but at the same resolution level. They do not look at satellites of dwarfs, nor do they run any UFDs, but in their sample of 15 haloes with $7.53 \times 10^9 < M_{\mathrm{halo}}/\mathrm{M}_{\odot} < 1.15 \times 10^{10}$, they form galaxies with a wide range of stellar masses, ranging up to $1.44 \times 10^7\,\mathrm{M}_{\odot}$. The lowest mass halo fails to form any stars at all. They tie this large scatter in $M_{\star}$ to the mass accretion history of the haloes, noting that the empty halo only very recently reached it's current halo mass through a major merger, and so was well below the mass at which SF suppression via the UV background is effective until recent times. With the exception of this particular halo, their stellar masses are in line with the results presented here for haloes of similar mass, lending further support to our claim of convergence at these particle masses.

The galaxies simulated in F17 have a range of SFHs, from early forming galaxies such as m10v to galaxies with later SF like m10q. Two of their haloes self-quench before $z = 0$ like our high-resolution version of m10q. They do not find a strong relationship between the $z = 0$ stellar masses and the timing of SF, but do find a correlation between the SFR and final $M_{\star}$, with higher mass galaxies forming stars at a faster rate. Although our sample is much smaller, at both resolution levels we find a similar correlation.

F17 also look at core formation in dwarf galaxies, finding cores only in galaxies with $M_{\star} > 2 \times 10^6\,\mathrm{M}_{\odot}$. With our much higher resolution, we are able to resolve our density profiles down to much lower radii (< 100 pc in all runs), and can therefore see small cores in galaxies (50–100 pc) with stellar masses below this cut-off. Our results for large (≳300 kpc) cores are consistent with their results. This ability to resolve particularly UFDs down to tens of pc is what allows us to predict the existence of small cores in these objects. Although they do not look at galaxies with $M_{\star} \lesssim 10^5\,\mathrm{M}_{\odot}$, they see similar results for their galaxies in the $M_{\star}$–$R_{1/2}$ plane as we present here. For a galaxy with $\sim 10^5\,\mathrm{M}_{\odot}$, they obtain $R_{1/2} \sim$

---

[13] O15 employ two different feedback prescriptions: one in which SN mass, momentum, and energy is deposited to the surrounding gas using a mass-weighting scheme and one that weights by volume of gas particles within the surrounding kernel. The current FIRE-2 weights this ejects by solid angle, but is much more similar to the volume-weighting prescription in O15 (Hopkins et al. 2018a for more details).

300 pc. Galaxies with $M_\star \sim 2 \times 10^6\,\mathrm{M}_\odot$ have a range of $R_{1/2}$ values from 500–800 pc, consistent with m10q at both resolution levels.

4.2 Simulations run with other codes

Revaz & Jablonka (2018, hereafter R18) run 27 zoom-in simulations of haloes with $5.4 \times 10^8\,\mathrm{M}_\odot \lesssim \mathrm{M}_{\rm vir} \lesssim 9.5 \times 10^9\,\mathrm{M}_\odot$ with GEAR, an SPH code based on GADGET-2, but with the Lagrangian 'pressure–entropy' formulation of the SPH equations, which fixes previous difficulties SPH codes had in modelling multiphase fluids (Agertz et al. 2007). These simulations are of lower resolution than ours, with $m^{\rm p}_{\rm DM} = 3.4 \times 10^4\,\mathrm{M}_\odot$, $m^{\rm p}_{\rm bar} = 1.5 \times 10^3\,\mathrm{M}_\odot$, $\mathrm{DM}_{\rm soft} = 50\,\mathrm{pc}$, and $\mathrm{g}_{\rm soft} = 10\,\mathrm{pc}$, which may explain why they get significantly higher stellar masses than we do for dwarfs with similar halo masses – their $M_{\rm halo} \sim 10^{10}\,\mathrm{M}_\odot$ haloes have $M_\star \gtrsim 4 \times 10^8\,\mathrm{M}_\odot$, a full two to three orders of magnitude larger than our haloes in the same mass range, and larger than all of the AM relations in Fig. 4. While 19 of their galaxies have $M_\star \lesssim 2 \times 10^6\,\mathrm{M}_\odot$, all of these galaxies form in $M_{\rm halo} \lesssim 3 \times 10^9\,\mathrm{M}_\odot$ haloes, haloes that form UFDs in our simulations. It is unclear what causes such a large difference between our results, but it could be a result of the resolution difference, or their much lower required density for SF $n_{\rm crit} > 1\,\mathrm{cm}^{-3}$.

R18 cite numerical heating as the cause of their $R_{1/2}$ values remaining constant at ~600 pc for galaxies with $10^5 \lesssim M_\star \lesssim 10^6\,\mathrm{M}_\odot$ – at the upper edge of the observed range. They strengthen this argument by plotting $R_{1/2}$ at the time the dwarf ceases forming stars, finding lower values better in line with observations. Due to the high stellar masses of these galaxies, they are resolved with several hundred stellar particles even at this low resolution, so this may counter our claim that our results are insensitive to numerical expansion. However, our $R_{1/2}$ values *increase* for higher resolution. An alternate explanation for the large $R_{1/2}$ values in R18 could be the low mass of the haloes (for their stellar mass). A velocity dispersion floor, as can be seen in their fig. 5 for galaxies in this same stellar mass range, combined with decreasing halo mass, can also lead to larger $R_{1/2}$ values (Bullock 2010).

The MZR found by R18 exhibits the same discrepancy with observations that we see for our highest mass galaxies ($M_\star \sim 10^5$–$10^6\,\mathrm{M}_\odot$). Many of their dwarfs in this mass range have $[\mathrm{Fe/H}] \lesssim -2.5$. They attribute this to the fact that the yields from their IMF do not vary in time nor with metallicity. This is the case for our simulations as well, and could lead to underpredicting [Fe/H], as it fails to allow for the possibility that higher mass stars disperse more metals into the ISM at early times. We will explore time- and metallicity-dependent yields in a future paper (Muley et al., in preparation).

Macciò et al. (2017, hereafter M17) use the SPH code GASOLINE (Wadsley, Stadel & Quinn 2004) to run a suite of 27 haloes with $5 \times 10^8 \lesssim M_{\rm vir}/\,\mathrm{M}_\odot \lesssim 10^{10}$ down to $z = 1$ in order to study the properties of dwarf galaxies before being accreted on to a host galaxy. Of these 27 haloes, five are run at their highest resolution of $m^{\rm p}_{\rm DM} = 600\,\mathrm{M}_\odot$, $m^{\rm p}_{\rm bar} = 119\,\mathrm{M}_\odot$, $\mathrm{DM}_{\rm soft} = 21\,\mathrm{pc}$, and $\mathrm{g}_{\rm soft} = 9\,\mathrm{pc}$. All haloes are run with $m^{\rm p}_{\rm bar} < 1000\,\mathrm{M}_\odot$ and $\mathrm{g}_{\rm soft} \leq 21\,\mathrm{pc}$. Eight of the galaxies remain completely dark at $z = 1$, while our simulated galaxies with $M_{\rm halo} > 5 \times 10^8\,\mathrm{M}_\odot$ all form at least 100 star particles (by redshift zero). The authors cite the cosmic ionizing background as the likely reason the haloes remain dark, showing in their fig. 4 that total gas fractions are consistent at a given stellar mass between haloes that form galaxies and those that do not, disfavouring feedback as the cause.

Interestingly, in M17, each of the galaxies that do form have at least $M_\star > 4 \times 10^4\,\mathrm{M}_\odot$, meaning that no galaxies form with fewer than ~150 star particles. This is in stark contrast to our simulations, which form many 'unresolved' galaxies with less than 100 star particles – many host only a single star particle. This could be due to their lower density requirement for SF – stars can form in gas with density $n_{\rm crit} > 60\,\mathrm{cm}^{-3}$, compared to our much more restrictive $n_{\rm crit} > 100$–$10^5\,\mathrm{cm}^{-3}$ – which may cause larger clusters of stars to form in the diffuse gas. In addition, the galaxies in M17 have a much larger $M_\star$ at a given halo mass than do the simulations presented here, even at $z = 1$. This may be because M17 only model SN feedback (i.e. they do not have a prescription for radiation pressure, local photo-ionizing radiation, or early stellar winds from massive stars), and so SNe are inefficient at expelling gas from high-density regions. Only two of the 19 galaxies that form are what we would call UFDs ($M_\star < 10^5\,\mathrm{M}_\odot$), and they form in two of the three lowest mass haloes ($M_{\rm halo} \lesssim 10^9\,\mathrm{M}_\odot$). Both if these galaxies have their SF shut down before $z = 6$, similar to our results.

Although their stellar masses are much larger than ours for a given halo mass, M17 also find a flattening of the inner slope of the dark matter density profile for galaxies with $M_\star \gtrsim 10^6\,\mathrm{M}_\odot$, but not at lower stellar mass. This is also consistent with Di Cintio et al. (2014a), who find that the dark matter profile steepens for $M_\star/M_{\rm halo} < 10^{-4}$. M17 also fail to match the observed MZR at $M_\star < 10^6\,\mathrm{M}_\odot$. They attribute this discrepancy to insufficient time resolution, meaning that the few bursts of SF that occur in their dwarfs do not have enough time to enrich the gas before the following burst of SF.

Munshi et al. (2019, hereafter M19) use CHANGA, a code based on GASOLINE, but with an improved SPH implementation that better handles the interface between hot and cold media. M19 use a previous suite of dwarf galaxies drawn from a cosmological 'sheet' in a single high-resolution region of a single simulation (Munshi et al. 2013). At the highest resolution, these simulations reach $m^{\rm p}_{\rm DM} = 6650\,\mathrm{M}_\odot$, $m^{\rm p}_{\rm bar} = 1410\,\mathrm{M}_\odot$, $\mathrm{DM}_{\rm soft} = 60\,\mathrm{pc}$, and $\mathrm{g}_{\rm soft} = 6\,\mathrm{pc}$. M19 run this entire zoom-in region with two different SF prescriptions: 'Metal Cooling (MC)' – where stars form in dense ($n_{\rm crit} > 100\,\mathrm{cm}^{-3}$) gas that falls below 10^4K, and 'Molecular Hydrogen (H2)' – where the SF efficiency scales with the fraction of molecular hydrogen in the baryonic particle (See M19 and Christensen et al. 2012 for more details).

M19 find a significant difference in the number of UFDs formed between the two runs, particularly among the satellites. The MC run forms five times as many satellites of more massive dwarfs as does the H2 run, and twice the number of dwarfs overall. They attribute this difference primarily to the fact that in the H2 run low-metallicity gas must reach extremely high densities ($n_{\rm crit} > 1000\,\mathrm{cm}^{-3}$) to cool – densities not possible in the MC run given the particle mass and softening lengths used, and that most low-mass haloes are unable to achieve before the ionizing background shuts down their SF. Galaxies in M19 have a large scatter in $M_{\rm halo}$ at a given $M_\star$; galaxies with $M_\star \sim 10^4\,\mathrm{M}_\odot$ can be hosted in haloes with $10^{6.5} \lesssim M_{\rm halo}/\,\mathrm{M}_\odot \lesssim 10^{8.8}$ (in the MC run). This 'flattening' of the $M_\star$–$M_{\rm halo}$ relation was also highlighted by Sawala et al. (2015), and could be a resolution effect, as it tends to occur at the stellar mass corresponding to a few-10 star particles (W15). It is worth pointing out that we do not see a flattening at the very-low-mass end of our $M_\star$–$M_{\rm halo}$ relation, although we do see greatly increased scatter. We will investigate this in an upcoming paper. Galaxies in M19 with $M_{\rm halo} \sim 10^{10}\,\mathrm{M}_\odot$ have slightly more stellar mass than our results, with values in the range 10^6–$10^8\,\mathrm{M}_\odot$, slightly higher in the H2 run for this mass range. This is likely due to the ability of the gas to self shield in this run. At the low-mass end, M19 form galaxies in dark matter haloes with $M_{\rm halo} \lesssim 10^7\,{\rm M}_\odot$. This is much lower than our low halo mass of $M_{\rm halo} \sim 5 \times 10^8\,{\rm M}_\odot$, but these are our 'resolved' galaxies – we form single star particles in haloes as low as $M_{\rm halo} \sim 10^6\,{\rm M}_\odot$.

M19 show cumulative SFHs for their dwarfs, but do not break them down by stellar mass. There is a population of dwarfs that have their SF shut down at an early time consistent with the onset of reionization, but a larger population have delayed SF – reionization prevents SF in these galaxies for a certain amount of time. The delayed SF occurs in both the MC and H2 runs, but is more pronounced in the M2 run. Although we have a much smaller sample, none of our dwarfs exhibit a delay in SF.

Agertz et al. (2019, hereafter A19) run the same $M_{\rm halo} = 10^9\,{\rm M}_\odot$ UFD with a variety of SF and feedback prescriptions, including several runs with full radiative transfer (RT), using the radiation hydrodynamic adaptive mesh refinement code RAMSES-RT (Rosdahl et al. 2013). At the highest resolution level, these simulations achieve $m^{\rm p}_{\rm DM} = 118\,{\rm M}_\odot$, $m^{\rm p}_{\rm bar} = 20\,{\rm M}_\odot$, and a mean spatial resolution of 3 pc in the ISM. Of all the runs, the run with full RT comes the closest to our stellar mass for a $M_{\rm halo} \sim 10^9\,{\rm M}_\odot$ halo, forming just over $10^4\,{\rm M}_\odot$ in stars – still a full order of magnitude more than in any of our lowest mass UFDs. The fact that the RT run comes the closest to our $M_\star$ values, and that their simulations without RT do not include a sub-grid mechanism for radiative feedback, suggests that feedback beyond SNe and stellar winds plays a non-trivial role in regulating SF at these masses.

A19 find half-mass radii that are consistent with the latest observational results (McConnachie 2012; Kirby et al. 2014; Simon 2019), as well as with the results presented here *for a given stellar mass*. As can be seen in their fig. 5, galaxies that form $\sim 10^4$–$10^5\,{\rm M}_\odot$ in stars have $R_{1/2} \sim 200$–300 pc. This is consistent with the results for our two galaxies in the same stellar mass range. However, at a given halo mass, our much lower $M_\star$ galaxies have two to three times larger $R_{1/2}$ values than the halo in A19, suggesting that the strong feedback in FIRE-2 not only leads to lower stellar masses, but to larger physical sizes at a given halo mass (e.g. El-Badry et al. 2016).

All of the fiducial models, with and without RT, from A19 have [Fe/H] values that are in line with observed values at the same *V*-band magnitude ($-2.7 \lesssim$ [Fe/H] $\lesssim -2.0$ for $-7 \lesssim M_{\rm V} \lesssim -5$; see their fig. 6), while our results have [Fe/H] $\lesssim -3.5$ for galaxies in the same stellar mass range. However, their simulations with increased SN energy lie nearly on top of our results, suggesting that the strong feedback in our simulations plays a role in regulating $M_\star$ which then sets [Fe/H]. Furthermore, in the few cases where A19 show the evolutionary tracks followed by a galaxy in the $M_{\rm V}$–[Fe/H] plane, the paths show that most of the galaxies had similarly low values of [Fe/H] when they had stellar masses similar to our lowest mass UFDs. This suggests that this problem may still exist in these simulations, and that the increased $M_\star$ is the primary factor in the ability for some of their runs to match observations.

5 CONCLUSIONS

We have run a suite of hydrodynamic cosmological zoom-in simulations with explicit treatment of SF and stellar feedback from SNe, stellar mass-loss, and radiation to $z = 0$. These simulations have baryonic mass resolution of $30\,{\rm M}_\odot$ (maximum resolved cold gas densities $\gtrsim 10^{5-6}\,{\rm M}_\odot$, spatial scales ~ 0.1–0.4 pc, time-scales $\sim$ 10–100 yr), allowing us to probe smaller physical scales than previously possible in cosmological simulations. They resolve ultra-faint dwarf galaxies ($M_\star < 10^5\,{\rm M}_\odot$) with $\gtrsim 100$–1000 star particles and, for the first time, the internal structure of individual SNe remnants within the cooling radius. Using these simulations, we have shown that:

(i) 'Well-resolved' galaxies ($\gtrsim 100$ star particles) exist in all DM haloes with $M_{\rm halo} > 5 \times 10^8\,{\rm M}_\odot$ or $V_{\rm max} > 13\ {\rm km\,s^{-1}}$. This suggests these are ubiquitous in the field. Using DM-only LG simulations, we estimate there are anywhere $\sim$180–380 such UFDs ($M_\star \sim 10^{3-5}\,{\rm M}_\odot$) 'isolated' in the Local Field, up to another $\sim$140 as satellites of other Local Field dwarfs, and $\sim$400–610 within the virial radii of the MW and Andromeda. However, we also predict most UFDs have very low surface brightness, below the detection capabilities of current surveys. It may be more efficient to search for UFDs as satellites of isolated LG field dwarfs: in the simulations, these have properties that may render them detectable by fully co-added LSST data.

(ii) All UFDs have uniformly ancient stellar populations: they complete SF by $z > 2$, even if they are isolated field centrals, owing to reionization quenching. More massive field dwarfs continue SF to $z < 0.5$.

(iii) Dwarfs in this mass range have bursty and strongly clustered SF in both time and space, which produces violent outflows. Despite this, only dwarfs with $M_\star/M_{\rm vir} \gtrsim 10^{-4}$ produce appreciable cores in their DM profiles; all the UFDs are below this threshold and exhibit DM cusps down to $\sim$100 pc or smaller (equivalent to $\sim 0.2\,R_{1/2}$). This is expected from simple energetic arguments: the UFDs simply produce insufficient stellar feedback to strongly perturb their DM potential. Neither the burstiness nor cusp/core threshold is strongly sensitive to resolution.

(iv) Properties that can be measured in lower resolution simulations (e.g. masses, sizes, cusp/core profiles, SFHs of the more massive galaxies here) appear robust to resolution, given the FIRE-2 numerical method adopted here. This is particularly important since many studies have argued the evolution of SNe blastwaves, bubble overlap, and galactic outflows becomes much less strongly sensitive to sub-grid numerical implementation choices at a mass resolution $< 100\,{\rm M}_\odot$ (owing to the ability to resolve individual SN blast waves self-consistently).

(v) Where the surface brightness is high enough to be detected, the simulations agree well with the location of observed galaxies in size-stellar mass-dynamical mass space. While there is a physical correlation between stellar size ($R_{1/2}$) and dynamical mass, driven by sampling a larger fraction of the halo mass at larger radii, there is no *intrinsic* tight correlation between stellar mass and size at these UFD masses. Rather, the observed relation reflects the surface-brightness limits of current surveys.

(vi) The simulations have $v_{\rm rot}/\sigma$ and ellipticity values consistent with most observed LG isolated and observed dwarfs. Both simulated and observed systems are primarily non-rotating, even in star-forming isolated field galaxies. Hints of discrepancies between rotation in observed and simulated FIRE dwarfs suggested in El-Badry et al. (2017, 2018) appear to manifest only at higher masses ($M_* \sim 10^{7-8}\,{\rm M}_\odot$).

(vii) Our dwarfs appear to underpredict the metallicities of observed LG satellites, with the discrepancy growing below $M_\star \ll 10^7\,{\rm M}_\odot$ to just under 2 dex for UFDs. We argue that some of this may owe to pre-enrichment in the LG environment by the massive host, suggesting the observed LG dwarfs may not be universally representative. It may also reflect our neglect of any treatment of Pop-III stars (a single one of which could, in theory, produce more than enough metals to account for the discrepancy), or more generally the effects of more detailed progenitor mass and metallicity-dependent yields.

Overall, our study confirms many results previously found in lower resolution simulations in the $M_\star \sim 10^3$–$10^6 M_\star$ mass scale. Given that these simulations are beginning to resolve the evolution of individual SNe, this suggests that the sub-grid approximations used in the lower resolution simulations may be robust, at least in so far as their consequences for galaxy properties. The major uncertainties at the resolution level simulated here may no longer lie in sub-grid treatments of the collective effects of stellar feedback (which can be explicitly resolved) but rather in the fact that different individual stars have different evolutionary histories and feedback properties. One hopes that this may signal a turning point in simulations of dwarfs where we move from cosmological simulations with effective or sub-grid ISM physics models to those that directly model collapse and fragmentation of molecular clouds into individual stars, akin to previous studies of first stars or the rich studies of individual patches of the ISM (which actually often contain more mass than a UFD).

ACKNOWLEDGEMENTS

CW is supported by the Lee A. DuBridge Postdoctoral Scholarship in Astrophysics. Support for PFH and SGK was provided by an Alfred P. Sloan Research Fellowship, NSF Collaborative Research Grant #1715847 and CAREER grant #1455342, and NASA grants NNX15AT06G, JPL 1589742, 17-ATP17-0214. ABP acknowledges generous support from the George P. and Cynthia Woods Institute for Fundamental Physics and Astronomy at Texas A&M University. SGK acknowledges additional support by NASA through Einstein Postdoctoral Fellowship grant number PF5-160136 awarded by the *Chandra* X-ray Center, which is operated by the Smithsonian Astrophysical Observatory for NASA under contract NAS8-03060. MBK acknowledges support from NSF grant AST-1517226 and CAREER grant AST-1752913 and from NASA grants NNX17AG29G and HST-AR-13888, HST-AR-13896, HST-AR-14282, HST-AR-14554, HST-AR-15006, HST-GO-12914, and HST-GO-14191 from the Space Telescope Science Institute, which is operated by AURA, Inc., under NASA contract NAS5-26555. AW received support from NASA, through ATP grant 80NSSC18K1097 and HST grants GO-14734 and AR-15057 from STScI, and a Hellman Fellowship from UC Davis. CAFG was supported by NSF through grants AST-1517491, AST-1715216, and CAREER award AST-1652522, by NASA through grants NNX15AB22G and 17-ATP17-0067, and by a Cottrell Scholar Award from the Research Corporation for Science Advancement. Numerical calculations were run on the Caltech compute cluster 'Wheeler,' allocations from XSEDE TG-AST130039 and PRAC NSF.1713353 supported by the NSF, and NASA HEC SMD-16-7592.

REFERENCES

Agertz O. et al., 2007, MNRAS, 380, 963
Agertz O. et al., 2019, preprint (arXiv:1904.02723)
Amorisco N. C., 2017, ApJ, 844, 64
Applebaum E., Brooks A. M., Quinn T. R., Christensen C. R., 2018, preprint (arXiv:e-prints)
Baushev A. N., Pilipenko S. V., 2018, preprint (arXiv:e-prints)
Bechtol K., et al., 2015, ApJ, 807, 50
Behroozi P. S., Wechsler R. H., Conroy C., 2013, ApJ, 770, 57
Binney J., 1978, MNRAS, 183, 501
Bovill M. S., Ricotti M., 2011a, ApJ, 741, 17
Bovill M. S., Ricotti M., 2011b, ApJ, 741, 18
Brook C. B., Di Cintio A., Knebe A., Gottlöber S., Hoffman Y., Yepes G., Garrison-Kimmel S., 2014, ApJ, 784, L14
Brown T. M. et al., 2014, ApJ, 796, 91
Bryan G. L., Norman M. L., 1998, ApJ, 495, 80
Buckley M. R., Peter A. H. G., 2018, Phys. Rep., 761, 1
Bullock J. S., 2010, preprint (arXiv:e-prints)
Bullock J. S., Boylan-Kolchin M., 2017, ARA&A, 55, 343
Bullock J. S., Kravtsov A. V., Weinberg D. H., 2000, ApJ, 539, 517
Bullock J. S., Stewart K. R., Kaplinghat M., Tollerud E. J., Wolf J., 2010, ApJ, 717, 1043
Caldwell N., Strader J., Sand D. J., Willman B., Seth A. C., 2017, Publ. Astron. Soc. Aust., 34, e039
Campbell D. J. R. et al., 2017, MNRAS, 469, 2335
Chan T. K., Kereš D., Oñorbe J., Hopkins P. F., Muratov A. L., Faucher-Giguère C.-A., Quataert E., 2015, MNRAS, 454, 2981
Chen K.-J., 2015, J. Phys.: Conf. Ser., 640, 012057
Christensen C., Quinn T., Governato F., Stilp A., Shen S., Wadsley J., 2012, MNRAS, 425, 3058
Cole A. A., Weisz D. R., Dolphin A. E., Skillman E. D., McConnachie A. W., Brooks A. M., Leaman R., 2014, ApJ, 795, 54
Collins M. L. M. et al., 2013, ApJ, 768, 172
de Blok W. J. G., 2010, Adv. Astron., 2010, 789293
de Blok W. J. G., Bosma A., 2002, A&A, 385, 816
Di Cintio A., Brook C. B., Macciò A. V., Stinson G. S., Knebe A., Dutton A. A., Wadsley J., 2014a, MNRAS, 437, 415
Di Cintio A., Brook C. B., Macciò A. V., Stinson G. S., Knebe A., Dutton A. A., Wadsley J., 2014b, MNRAS, 437, 415
Dijkstra M., Haiman Z., Rees M. J., Weinberg D. H., 2004, ApJ, 601, 666
Dooley G. A., Peter A. H. G., Yang T., Willman B., Griffen B. F., Frebel A., 2017, MNRAS, 471, 4894
Drlica-Wagner A. et al., 2015, ApJ, 813, 109
Efstathiou G., 1992, MNRAS, 256, 43P
Eisenstein D. J. et al., 2005, ApJ, 633, 560
El-Badry K., Wetzel A., Geha M., Hopkins P. F., Kereš D., Chan T. K., Faucher-Giguère C.-A., 2016, ApJ, 820, 131
El-Badry K., Wetzel A. R., Geha M., Quataert E., Hopkins P. F., Kereš D., Chan T. K., Faucher-Giguère C.-A., 2017, ApJ, 835, 193
El-Badry K., Weisz D. R., Quataert E., 2017, MNRAS, 468, 319
El-Badry K. et al., 2018, MNRAS, 473, 1930
Errani R., Peñarrubia J., Walker M. G., 2018, MNRAS, 481, 5073
Escala I. et al., 2018, MNRAS, 474, 2194
Faucher-Giguère C.-A., 2018, MNRAS, 473, 3717
Faucher-Giguère C.-A., Lidz A., Zaldarriaga M., Hernquist L., 2009, ApJ, 703, 1416
Fillingham S. P., Cooper M. C., Boylan-Kolchin M., Bullock J. S., Garrison-Kimmel S., Wheeler C., 2018, MNRAS, 477, 4491
Fitts A. et al., 2017, MNRAS, 471, 3547
Flores R. A., Primack J. R., 1994, ApJ, 427, L1
François P., Matteucci F., Cayrel R., Spite M., Spite F., Chiappini C., 2004, A&A, 421, 613
Garrison-Kimmel S., Rocha M., Boylan-Kolchin M., Bullock J. S., Lally J., 2013, MNRAS, 433, 3539
Garrison-Kimmel S., Boylan-Kolchin M., Bullock J. S., Lee K., 2014, MNRAS, 438, 2578
Garrison-Kimmel S. et al., 2017, MNRAS, 471, 1709
Garrison-Kimmel S., et al., 2019, MNRAS, 487, 1380
Geha M., Blanton M. R., Yan R., Tinker J. L., 2012, ApJ, 757, 85
González-Samaniego A., Bullock J. S., Boylan-Kolchin M., Fitts A., Elbert O. D., Hopkins P. F., Kereš D., Faucher-Giguère C.-A., 2017, MNRAS, 472, 4786
Governato F. et al., 2012, MNRAS, 422, 1231
Graus A. S., Bullock J. S., Kelley T., Boylan-Kolchin M., Garrison-Kimmel S., Qi Y., 2019, MNRAS, 488, 4585
Grudić M. Y., Hopkins P. F., 2019 , MNRAS, 488, 2970
Gunn J. E., Gott J. R., III, 1972, ApJ, 176, 1
Hoeft M., Yepes G., Gottlöber S., Springel V., 2006, MNRAS, 371, 401
Homma D. et al., 2016, ApJ, 832, 21

Homma D. et al., 2018, PASJ, 70, S18

Hopkins P. F., 2014, preprint (arXiv:e-prints)

Hopkins P. F., Kereš D., Oñorbe J., Faucher-Giguère C.-A., Quataert E., Murray N., Bullock J. S., 2014, MNRAS, 445, 581

Hopkins P. F. et al., 2018a, MNRAS, 477, 1578

Hopkins P. F. et al., 2018b, MNRAS, 480, 800

Hu C.-Y., 2018, MNRAS, 475, 4396

Jaacks J., Thompson R., Finkelstein S. L., Bromm V., 2018, MNRAS, 475, 4396

Karachentsev I. D. et al., 2001, A&A, 379, 407

Karachentsev I. D., Tully R. B., Wu P.-F., Shaya E. J., Dolphin A. E., 2014, ApJ, 782, 4

Karachentsev I. D., Makarova L. N., Makarov D. I., Tully R. B., Rizzi L., 2015, MNRAS, 447, L85

Kaufmann T., Wheeler C., Bullock J. S., 2007, MNRAS, 382, 1187

Keller B. W., Wadsley J. W., Wang L., Kruijssen J. M. D., 2019, MNRAS, 482, 2244

Kim C.-G., Ostriker E. C., 2015, ApJ, 802, 99

Kirby E. N., Martin C. L., Finlator K., 2011, ApJ, 742, L25

Kirby E. N., Boylan-Kolchin M., Cohen J. G., Geha M., Bullock J. S., Kaplinghat M., 2013a, ApJ, 770, 16

Kirby E. N., Cohen J. G., Guhathakurta P., Cheng L., Bullock J. S., Gallazzi A., 2013b, ApJ, 779, 102

Kirby E. N., Bullock J. S., Boylan-Kolchin M., Kaplinghat M., Cohen J. G., 2014, MNRAS, 439, 1015

Klypin A., Kravtsov A. V., Valenzuela O., Prada F., 1999, ApJ, 522, 82

Knollmann S. R., Knebe A., 2009, ApJS, 182, 608

Komatsu E. et al., 2011, ApJS, 192, 18

Kozyreva A., Yoon S.-C., Langer N., 2014, A&A, 566, A146

Kravtsov A. V., 2013, ApJ, 764, L31

Kroupa P., 2002, Science, 295, 82

Lapi A., Cavaliere A., Menci N., 2005, ApJ, 619, 60

Leitherer C. et al., 1999, ApJS, 123, 3

Ma X., Kasen D., Hopkins P. F., Faucher-Giguère C.-A., Quataert E., Kereš D., Murray N., 2015, MNRAS, 453, 960

Ma X., Hopkins P. F., Feldmann R., Torrey P., Faucher-Giguère C.-A., Kereš D., 2017a, MNRAS, 466, 4780

Ma X., Hopkins P. F., Wetzel A. R., Kirby E. N., Anglés-Alcázar D., Faucher-Giguère C.-A., Kereš D., Quataert E., 2017b, MNRAS, 467, 2430

Macciò A. V., Frings J., Buck T., Penzo C., Dutton A. A., Blank M., Obreja A., 2017, MNRAS, 472, 2356

Makarov D., Makarova L., Sharina M., Uklein R., Tikhonov A., Guhathakurta P., Kirby E., Terekhova N., 2012, MNRAS, 425, 709

Makarova L. N., Makarov D. I., Karachentsev I. D., Tully R. B., Rizzi L., 2017, MNRAS, 464, 2281

Martin N. F. et al., 2015, ApJ, 804, L5

Martizzi D., Faucher-Giguère C.-A., Quataert E., 2015, MNRAS, 450, 504

Mashchenko S., Couchman H. M. P., Wadsley J., 2006, Nature, 442, 539

McConnachie A. W., 2012, AJ, 144, 4

Moore B., 1994, Nature, 370, 629

Moore B., Ghigna S., Governato F., Lake G., Quinn T., Stadel J., Tozzi P., 1999, ApJ, 524, L19

Moster B. P., Naab T., White S. D. M., 2013, MNRAS, 428, 3121

Mo H. J., Mao S., White S. D. M., 1998, MNRAS, 295, 319

Munshi F. et al., 2013, ApJ, 766, 56

Munshi F., Brooks A. M., Applebaum E., Weisz D. R., Governato F., Quinn T. R., 2017, preprint (arXiv:e-prints)

Munshi F., Brooks A. M., Christensen C., Applebaum E., Holley-Bockelmann K., Quinn T. R., Wadsley J., 2019, ApJ, 874, 40

Muratov A. L., Kereš D., Faucher-Giguère C.-A., Hopkins P. F., Quataert E., Murray N., 2015, MNRAS, 454, 2691

Navarro J. F., Frenk C. S., White S. D. M., 1997, ApJ, 490, 493

Oh S.-H., de Blok W. J. G., Walter F., Brinks E., Kennicutt R. C., Jr, 2008, AJ, 136, 2761

Oñorbe J., Boylan-Kolchin M., Bullock J. S., Hopkins P. F., Kereš D., Faucher-Giguère C.-A., Quataert E., Murray N., 2015, MNRAS, 454, 2092

Planck Collaboration XVI, 2014, A&A, 571, A16

Pontzen A., Governato F., 2012, MNRAS, 421, 3464

Power C., Navarro J. F., Jenkins A., Frenk C. S., White S. D. M., Springel V., Stadel J., Quinn T., 2003, MNRAS, 338, 14

Read J. I., Agertz O., Collins M. L. M., 2016a, MNRAS, 459, 2573

Read J. I., Iorio G., Agertz O., Fraternali F., 2016b, MNRAS, 462, 3628

Read J. I., Iorio G., Agertz O., Fraternali F., 2017, MNRAS, 467, 2019

Reid B. A. et al., 2010, MNRAS, 404, 60

Revaz Y., Jablonka P., 2018, A&A, 616, A96

Ricotti M., Gnedin N. Y., 2005, ApJ, 629, 259

Rodriguez Wimberly M. K., Cooper M. C., Fillingham S. P., Boylan-Kolchin M., Bullock J. S., Garrison-Kimmel S., 2019, MNRAS, 483, 3031

Rosdahl J., Blaizot J., Aubert D., Stranex T., Teyssier R., 2013, MNRAS, 436, 2188

Salucci P., Burkert A., 2000, ApJ, 537, L9

Sawala T. et al., 2014, preprint (arXiv:e-prints)

Sawala T. et al., 2015, MNRAS, 448, 2941

Simon J. D., 2019, ARA&A, 57, 375

Sparre M., Hayward C. C., Feldmann R., Faucher-Giguère C.-A., Muratov A. L., Kereš D., Hopkins P. F., 2017, MNRAS, 466, 88

Su K.-Y., Hayward C. C., Hopkins P. F., Quataert E., Faucher-Giguère C.-A., Kereš D., 2018a, MNRAS, 473, L111

Su K.-Y. et al., 2018b, MNRAS, 480, 1666

Tollet E. et al., 2016, MNRAS, 456, 3542

Torrealba G. et al., 2019, MNRAS, 488, 2743

Tulin S., Yu H.-B., 2018, Phys. Rep., 730, 1

van den Bosch F. C., Dalcanton J. J., 2000, ApJ, 534, 146

van Dokkum P. G., Abraham R., Merritt A., Zhang J., Geha M., Conroy C., 2015, ApJ, 798, L45

Vargas L. C., Geha M. C., Tollerud E. J., 2014, ApJ, 790, 73

Viel M., Becker G. D., Bolton J. S., Haehnelt M. G., Rauch M., Sargent W. L. W., 2008, Phys. Rev. Lett., 100, 041304

Wadsley J. W., Stadel J., Quinn T., 2004, New Astron., 9, 137

Walch S., Naab T., 2015, MNRAS, 451, 2757

Weinmann S. M., Macciò A. V., Iliev I. T., Mellema G., Moore B., 2007, MNRAS, 381, 367

Wetzel A. R., Hopkins P. F., Kim J.-h., Faucher-Giguère C.-A., Kereš D., Quataert E., 2016, ApJ, 827, L23

Wheeler C., Oñorbe J., Bullock J. S., Boylan-Kolchin M., Elbert O. D., Garrison-Kimmel S., Hopkins P. F., Kereš D., 2015, MNRAS, 453, 1305

Wheeler C. et al., 2017, MNRAS, 465, 2420

Wolf J., Martinez G. D., Bullock J. S., Kaplinghat M., Geha M., Muñoz R. R., Simon J. D., Avedo F. F., 2010, MNRAS, 406, 1220

Woosley S. E., Weaver T. A., 1995, ApJS, 101, 181

York D. G. et al., 2000, AJ, 120, 1579

This paper has been typeset from a TEX/LATEX file prepared by the author.